AD

TECHNICAL REPORT BRL-TR-2786

LARGE BLAST-WAVE SIMULATORS (LBS) WITH COLD-GAS DRIVERS: COMPUTATIONAL DESIGN STUDIES

KLAUS O. OPALKA

MARCH 1987

US ARMY BALLISTIC RESEARCH LABORATORY
ABERDEEN PROVING GROUND, MARYLAND

Destroy this report when it is no longer needed.
Do not return it to the originator.

Additional copies of this report may be obtained from the National Technical Information Service, U. S. Department of Commerce, Springfield, Virginia 22161.

The findings in this report are not to be construed as an official Department of the Army position, unless so designated by other authorized documents.

The use of trade names or manufacturers' names in this report does not constitute indorsement of any commercial product.

UNCLASSIFIED
SECURITY CLASSIFICATION OF THIS PAGE

AD-A181 400

REPORT DOCUMENTATION PAGE

Form Approved
OMB No. 0704-0188
Exp. Date: Jun 30, 1986

1a. REPORT SECURITY CLASSIFICATION: UNCLASSIFIED	1b. RESTRICTIVE MARKINGS: NONE
2a. SECURITY CLASSIFICATION AUTHORITY	3. DISTRIBUTION/AVAILABILITY OF REPORT
2b. DECLASSIFICATION/DOWNGRADING SCHEDULE	
4. PERFORMING ORGANIZATION REPORT NUMBER(S): TECHNICAL REPORT BRL-TR-	5. MONITORING ORGANIZATION REPORT NUMBER(S)
6a. NAME OF PERFORMING ORGANIZATION: US ARMY BALLISTIC RESEARCH LABORATORY; 6b. OFFICE SYMBOL (If applicable): SLCBR-TB-B	7a. NAME OF MONITORING ORGANIZATION
6c. ADDRESS (City, State, and ZIP Code): ABERDEEN PROVING GROUND, MD 21005-5066	7b. ADDRESS (City, State, and ZIP Code)
8a. NAME OF FUNDING/SPONSORING ORGANIZATION: US ARMY HARRY DIAMOND LABORATORY; 8b. OFFICE SYMBOL (If applicable): SLCHD-NW-P	9. PROCUREMENT INSTRUMENT IDENTIFICATION NUMBER
8c. ADDRESS (City, State, and ZIP Code): 2800 POWDER MILL ROAD, ADELPHI, MD 20783-1197	10. SOURCE OF FUNDING NUMBERS: PROGRAM ELEMENT NO. 62120; PROJECT NO. AH25; TASK NO.; WORK UNIT ACCESSION NO.

11. TITLE (Include Security Classification): LARGE BLAST-WAVE SIMULATORS (LBS) WITH COLD-GAS DRIVERS: COMPUTATIONAL DESIGN STUDIES

12. PERSONAL AUTHOR(S): KLAUS O. OPALKA

13a. TYPE OF REPORT	13b. TIME COVERED	14. DATE OF REPORT (Year, Month, Day)	15. PAGE COUNT
FINAL	FROM _____ TO FY86		

16. SUPPLEMENTARY NOTATION

17. COSATI CODES			18. SUBJECT TERMS (Continue on reverse if necessary and identify by block number)
FIELD	GROUP	SUB-GROUP	
20	04		LARGE BLAST-WAVE SIMULATORS; LBS-DESIGN STUDIES; SHOCK TUBES W/VARIABLE CROSS-SECTIONAL AREAS; SHOCK TUBES; BLAST-WAVE SIMULATION

19. ABSTRACT (Continue on reverse if necessary and identify by block number)

Computational, parametric design studies were carried out using the BRL-Q1D hydrocode to investigate the effects of variations in length of a US-LBS designed to simulate blast waves within a predefined test envelope. The simulation requirement was based on a $60m/kT^{1/3}$ Height-of-Burst, scaled, tactical explosion for shock overpressures ranging from 14 to 240 kPa (2-35 psi) and weapon yields ranging from 1 kT to 1 MT.

The US-LBS design is based on the LBS at the Centre d'Etudes de Gramat (CEG), France. However, the cross-sectional reference area of the test section is expected to be twice the size of the French facility. Studies are preformed to investigate the effects of changes of the driver length, the expansion-tube length without RWE and the expansion-tube length with a passive RWE. The results of these studies are presented in form of design envelopes, and discussed. Recommendations are made fro the US-LBS design.

Keywords:

20. DISTRIBUTION/AVAILABILITY OF ABSTRACT	21. ABSTRACT SECURITY CLASSIFICATION
☒ UNCLASSIFIED/UNLIMITED ☐ SAME AS RPT. ☐ DTIC USERS	UNCLASSIFIED

22a. NAME OF RESPONSIBLE INDIVIDUAL	22b. TELEPHONE (Include Area Code)	22c. OFFICE SYMBOL
Klaus O. Opalka	(301) 278-6036	SLCBR-TB-B

DD FORM 1473, 84 MAR — 83 APR edition may be used until exhausted. All other editions are obsolete.

SECURITY CLASSIFICATION OF THIS PAGE
UNCLASSIFIED

ITEM 18 (continued):

BLAST WAVES;
SHOCK OVERPRESSURE;
PRESSURE HISTORY;
DYNAMIC PRESSURE ;
COMPUTATIONAL FLUID DYNAMICS;
HYDROCODE COMPUTATIONS;
BRL-Q1D CODE

TABLE OF CONTENTS

LIST OF ILLUSTRATIONS

1. INTRODUCTION

The ban on above-ground nuclear testing forces the U. S. Army to look for alternative techniques in its effort to meet the growing need for nuclear, blast/thermal survivability testing of military equipment. There are currently two techniques used to simulate the blast effects of nuclear explosions involving either high explosives in large quantities, or special shock tubes. The simulation of nuclear blasts with high explosives (HE) is very costly and limited to small yields ($\leq$20 kT). HE tests require large test areas and their set-up is time consuming. For these reasons, the use of specialized shock tubes is becoming increasingly attractive. Such facilities, called large blast-wave simulators (LBS), are large enough to accommodate full-sized tactical equipment such as trucks, tanks and helicopters. A few LBS facilities exist abroad, the largest at the Centre d'Etudes de Gramat (CEG) in France,[1*] but none is located on the North-American continent.

The U. S. Army, in concert with other government agencies, is presently developing a concept of such a facility suitable to simulate both thermal and blast effects of nuclear explosions for the survivability testing of military equipment and for research studies. Blast waves will be simulated by releasing compressed gas from several drivers of varying length into a large expansion tunnel constructed of pre-stressed concrete. The thermal simulation will be effected through aluminum/oxygen combustion near the target. The conditions being simulated correspond to those produced by a tactical nuclear air burst with a scaled height of burst of $60m \times W^{1/3}$, i.e the height is equal to 60 metres times the weapon yield in kilotons taken to the 1/3 power. A simulated blast wave is said to approximate a given free-field blast wave if the peak overpressure, the impulse and the initial rate of overpressure decay correspond to the free-field parameters associated with the given yield and shock overpressure.

The current US design studies are based on the Large Blast Simulator at the Center d'Etudes de Gramat (CEG), France. However, studies of the effect of target blockage on target loading[2] indicate that a much larger facility would be needed in order to accommodate the full range of anticipated targets. The studies will also be extended over a broad range of shock overpressures and weapon yields to cover test conditions which cannot be simulated in the CEG facility. Therefore, a parametric study was initiated to answer questions about the necessary size and the expected performance of such a facility. A numerical approach seemed preferable to an experimental one, because the latter would have taken up too much preparation time and yielded only few data points. On the other hand, numerical methods for solving the Euler equations already existed and an implicit, factored finite-difference scheme[3] was chosen to develop the quasi-one-dimensional BRL-Q1D code[4,5] for simulating the flow in blast-wave simulators.

This report presents the results of computational, parametric design studies which have as their goal the definition of the necessary variations of length of the driver assembly and of the expansion tube as a function of the shock overpressure and of the weapon yield at a given test station. A passive rarefaction-wave eliminator (RWE) is considered in lieu of a very long expansion tube. The LBS characterization is presented in chapter 3, and the implications for an US-LBS design are discussed in chapter 4. Finally, our conclusions are presented in chapter 5. The LBS concept and associated physical flow phenomena are discussed in the next chapter.

---

* *references are listed at the end of the report*

2. THE LBS CONCEPT

Large blast-wave simulators are basically shock tubes whose cross-sectional areas vary along their lengths. They are designed to produce decaying blast waves akin to those which are generated by nuclear explosions.[6] In this chapter, we discuss the major concepts of an LBS facility and its physical flow phenomena.

2.1 THE FRENCH LBS

The present studies are based on the design features of the French LBS at the CEG. The basic layout of the CEG facility is shown in Figure 1. The drivers provide high-pressure air for the production of the blast wave. The convergent-divergent nozzles contain the diaphragm assembly in the throat section; they basically serve to retard the emptying of the drivers. The expansion tube receives the expanding gas and guides it through the test section, which is located about seven diameters downstream from the nozzle exits. The RWE at the open end prevents the formation of rarefaction waves which would travel upstream and disturb the blast-wave simulation in the test section.

Because of the considerable size of this facility, a single driver with a single diaphragm would be impractical. Therefore, the shock wave in the expansion tube is driven by an array of seven steel driver tubes each 1.33 metres in diameter. For wave-shaping purposes, the drivers have different lengths of 19 metres (2 drivers), 26 metres (2 drivers), 35 metres (1 driver) and 44 metres (2 drivers). Each driver is connected to an 11 metres long, convergent-divergent nozzle. The convergent nozzle connects the driver cylinder to the throat section reducing the diameter to 0.665 metres. The throat section is followed by a divergent nozzle which extends into the expansion tube with a 6° half-angle cone.

The diaphragms are mounted in removable holders, which form a part of the throat section ahead of the convergent nozzle. The holders are fully interchangeable in order to facilitate easy installation after replacing the spent diaphragm. The diaphragms are made of mild steel and either flat or hemispherically prestressed if that is required by a high driver pressure. All seven diaphragms are opened simultaneously by detonating thin explosive strips, called cutting charges, which are mounted on the downstream faces of the diaphragms.

The expansion tube is built of pre-stressed concrete and is 105 metres long. It overlaps the divergent nozzles at the upstream end for about one metre. The upper half of the tube resembles closely a circular arch of 6.2 metres inner radius. The sides are formed by two vertical walls, 2.46 metres high. The width of the expansion tube is 12 metres at the ground floor level. The test section is located 60 metres downstream from the exit of the divergent nozzles and is 15 metres long. The length preceding the test section is a smoothing zone needed to establish uniform flow over the cross-section of the expansion tube. The walls of the test section are equipped with a large number of ports for cameras, lighting and instrumentation. A safety zone of 30 metres behind the test section provides space for the displacement of targets. An underground access tunnel runs the whole length of the expansion tube.

The RWE at the open end of the expansion tube consists of a system of rotating shutters which are opened and closed by a system of hydraulic jack screws linked mechanically to the shutters. The hydraulic jacks are driven by electric motors the motions of which are pre-programed by an electronic control unit. During the operation of the LBS, the RWE is attached to the expansion tube with 18 anchors along the periphery of the tube. In the fully-open position, the RWE structure obstructs only 5% of the cross-sectional area of the expansion tube.

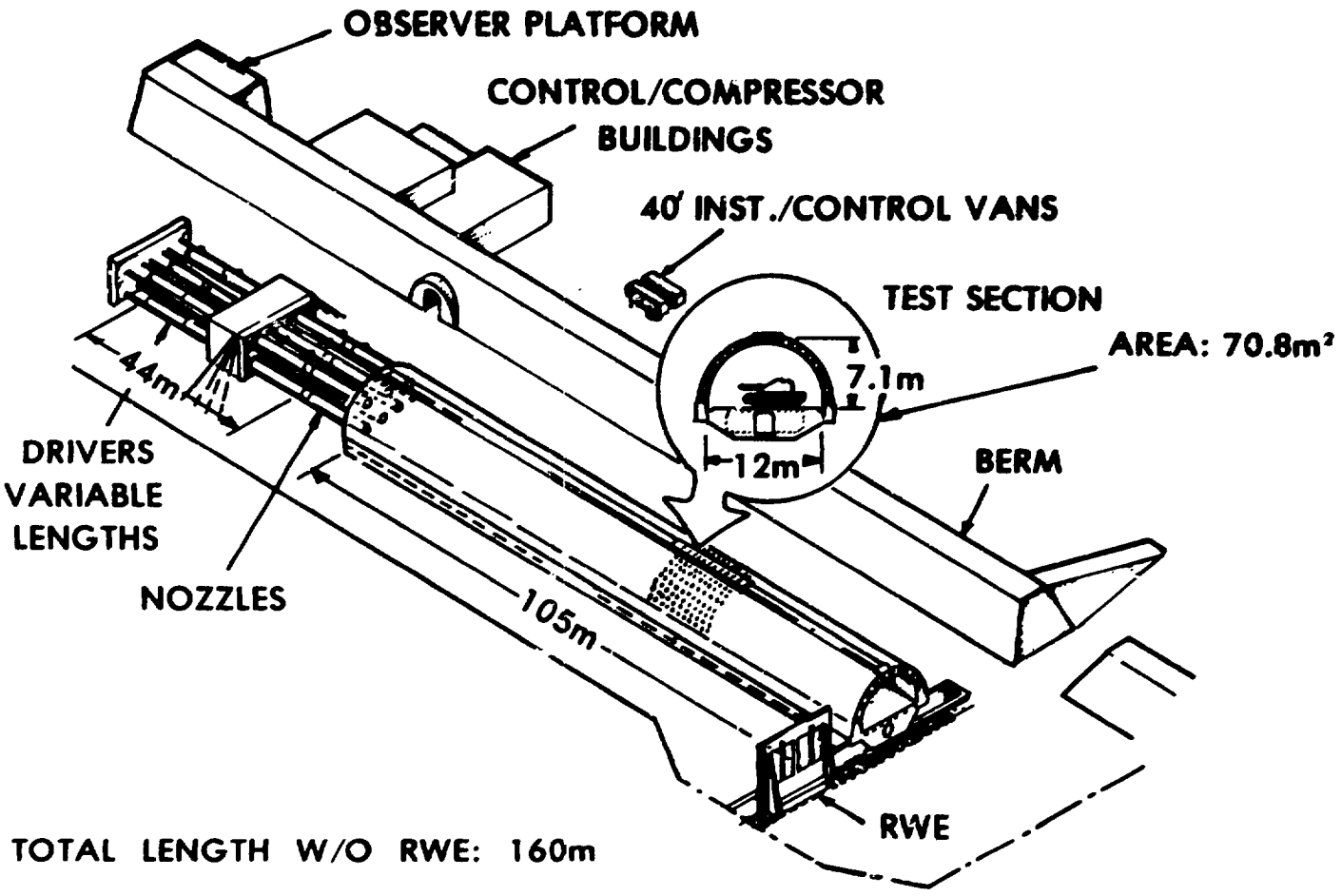

Figure 1: The LBS at the Centre d'Etudes de Gramat, France.

2.2 THE LBS OPERATION

The operation of the LBS includes several phases,[1] such as the instrumentation of the target in the test section, the calibrating of recording instrumentation in the data acquisition center, the programming of the RWE, the installation of diaphragms and cutting charges, and the pressurization of the drivers. After final safety checks are performed, the firing sequence is initiated. The cutting charges open the diaphragms and the high-pressure gas in the drivers is released. The gas flows out through the nozzles and forms a shock wave. The shock wave moves down the expansion tube and starts the blast loading of the target. Behind the shock front, the static overpressure decays in a fashion similar to that observed in a free-field blast wave. At the end of the expansion tube the shock interacts with the RWE.

The RWE partially reflects the incident shock and generates a rarefaction wave which interacts with the reflected shock to cancel each other. The RWE then begins to close such that this interaction continues preventing any flow disturbance from moving upstream into the test section. Finally, rarefaction waves generated in the drivers move through the test section lowering the pressure and decelerating the flow. The simulation ends when the overpressure returns to the ambient condition.

2.3 FLOW PHENOMENA IN AN LBS

The flow patterns encountered in an LBS are much more complex than those encountered in a straight shock tube. Figure 2a shows a schematic comparison of the flow patterns in a straight shock tube and in a blast-wave simulator. The initial flow pattern in a straight shock tube is made up of a primary shock (2) moving into ambient air (1), followed by a contact surface (3) which separates the hot gas processed by the shock from the cold gas initially in the driver (4). A rearward facing rarefaction wave in the driver (5) accelerates and cools the driver gas. For low shock overpressures (e.g. < 28 kPa for the French LBS), the flow in an LBS is similar to that in a straight shock tube in that it is subsonic everywhere with a steady expansion in the convergent nozzle and a steady compression in the divergent nozzle.

Generally, the flow in an LBS is distinguished from the flow in a conventional shock tube by the occurrance of choked flow in the throat of the nozzle (7), and a recompression shock (10) compensating for the supersonic expansion of the flow in the divergent nozzle (8). As the driver empties, the subsonic flow expands isentropically in the convergent nozzle (6) such that it becomes sonic in the throat. The flow then becomes supersonic as it continues to expand in the divergent nozzle; but because the flow behind the primary shock (2) is subsonic, a recompression shock (10) must form to decelerate the supersonic flow to match the velocity across the contact surface (3).

For moderate shock overpressures (e.g. 28 - 70 kPa for the French LBS), the flow forms a standing shock part way through the divergent nozzle. The subsonic flow behind it goes through a steady compression in the remaining part of the nozzle. For high shock overpressures (e.g. > 70 kPa for the French LBS), the recompression shock is swept out of the nozzle and down the expansion tube (see Figure 2b). It is followed by a region of supersonic flow at extremely low pressure. In extreme cases, the recompression shock may be swept past the test section, and the low-pressure region behind it destroys the blast-wave simulation. At later times, the recompression shock returns to the nozzle exit where it is partially reflected (16) and partially transmitted (13) moving upstream into the drivers.

Late-time wave patterns are illustrated in Figure 2a and 2b, also. The decay of static and dynamic pressure necessary for the simulation of a blast wave is produced by rarefaction waves which are reflected from the closed ends of the drivers (14). Moving forward, the rarefactions interact with the convergent nozzle and are partially transmitted and partially

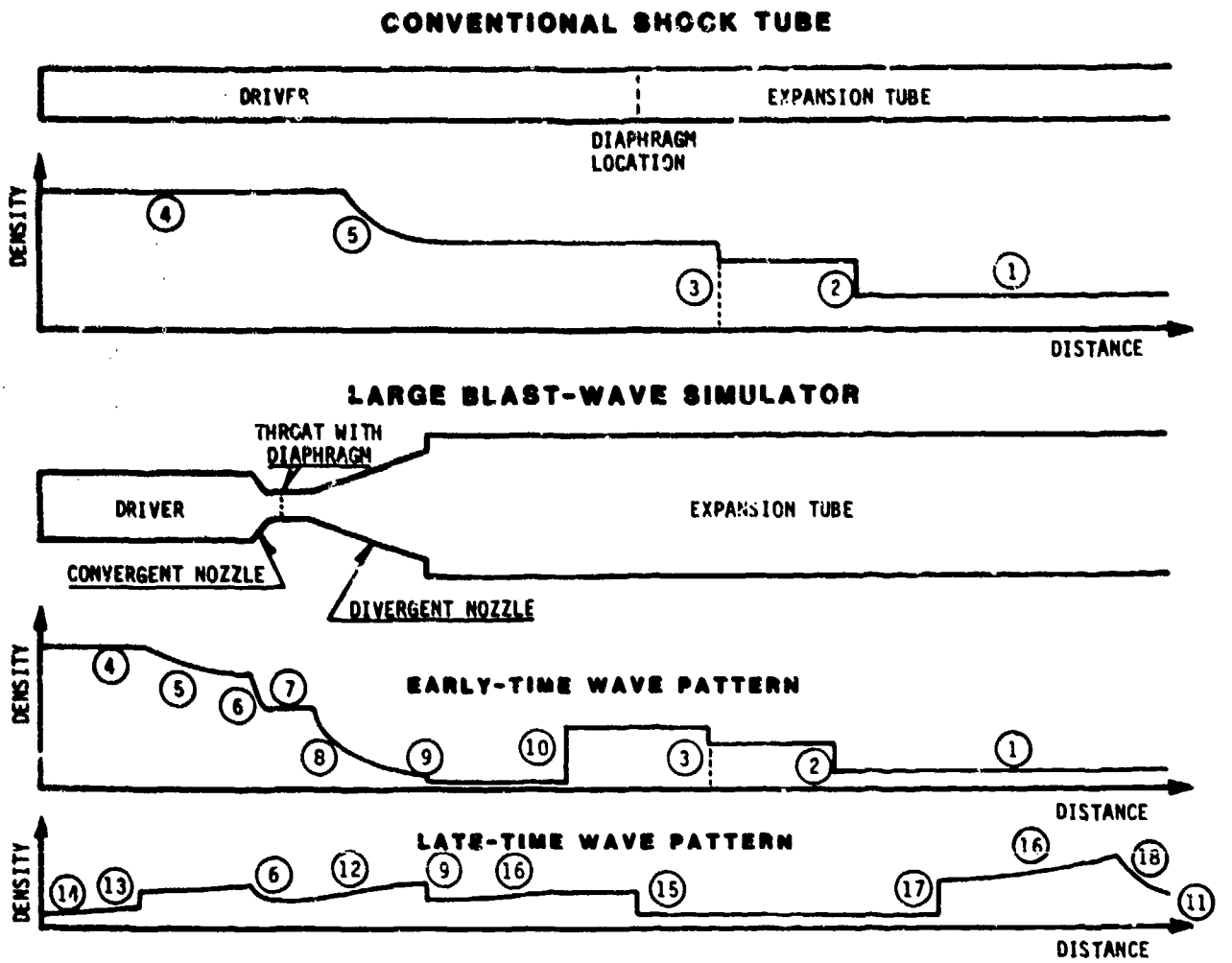

LEGEND

EARLY-TIME FLOW PATTERN		LATE-TIME FLOW PATTERN	
1	Ambient Conditions	11	Outflow at Ambient Pressure
2	Principal Shock	12	Isentropic Compression of Subsonic Flow
3	Contact Surface	13	Recompression Shock Partially Transmitted into Drivers
4	Initial Driver Conditions	14	Rarefaction Wave Reflected from Driver End
5	Rarefaction Wave	15	Recompression Shock Partially Reflected from Nozzle Exit
6	Isentropic Expansion of Subsonic Flow	16	Rarefaction Wave Transmitted through Nozzle
7	Choked Flow in Throat	17	Back-Facing Shock from Open End of Expansion Tube
8	Isentropic Expansion of Supersonic Flow	18	Rarefaction Wave from Open End of Expansion Tube
9	Density Discontinuity at Nozzle Exit		
10	Recompression Shock		

(a) Typical Wave Patterns

Figure 2: Illustration of Physical Flow Phenomena.

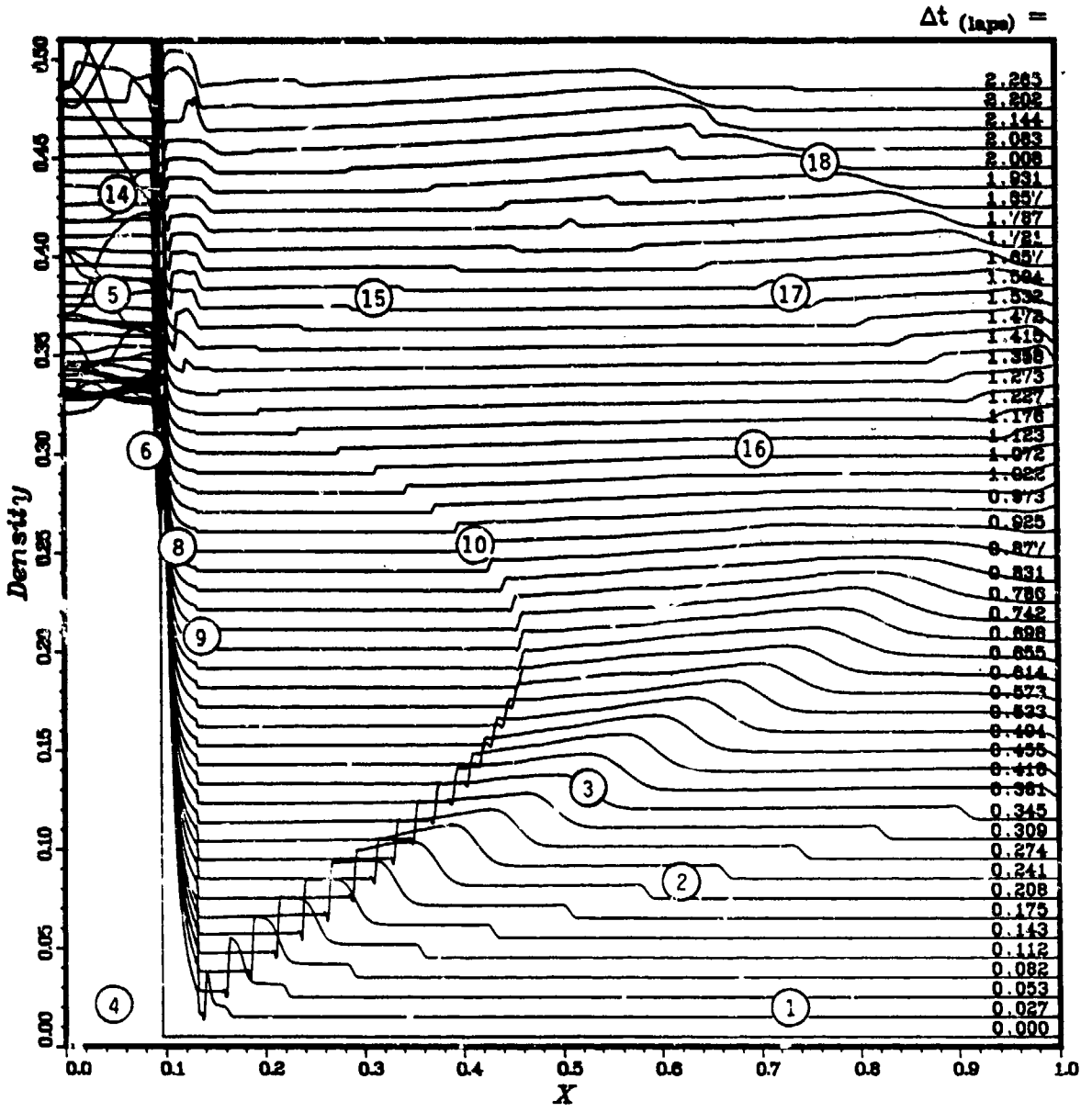

(b) Computational Explication

Figure 2: (concluded)

reflected. The transmitted parts of the rarefactions (15) overtake the shock at different times because the drivers are of different lengths, and decrease its strength. The parts of the rarefactions which are reflected from the convergent nozzles move back into the drivers and are again reflected from the closed ends of the drivers.

In the absence of an active RWE, rarefactions also proceed upstream from the open end of the expansion tube after the incident shock has exited (18), and a back-facing shock from the open end (17) brings the overexpanded driver gas back to ambient pressure. Thus series of rarefaction waves and shocks move up and down the expansion tube restoring the ambient conditions. Figure 2b gives a fine example of the wave patterns in an LBS gained from a quasi-one-dimensional computation. Many of the discussed details are recognizable in this graph of density versus distance although it is hard to see what is hapening in the driver. Another plot showing the driver on a larger scale has not been helpful in untangling the lines because of the great density oscillations occurring in the driver.

3. COMPUTATIONAL LBS CHARACTERIZATION

The purpose of the present studies is to investigate the variations in length of the drivers and of the expansion tube which will be necessary to design a US-LBS facility capable of operating over a required range of weapon yields and overpressures greater than that of the CEG facility. The dimensions of the CEG facility are used as basis for the comparison. The BRL-Q1D code[4] is an efficient tool for these parametric studies because of its short execution times. It has been shown to predict the flow in blast-wave simulators with sufficient accuracy although there are limitations to the predictions due to the one-dimensional approach.

3.1 THE QUASI-ONE-DIMENSIONAL LBS MODEL

The computational LBS model of the CEG facility is shown in Figure 3. The seven drivers are combined into one by lumping the cross-sectional areas at any given location into a single area. The stair-stepped driver results. The four steps indicate that the French facility incorporates drivers of four different lengths. In the same manner, the areas of the seven nozzles are lumped into one. The RWE is modelled computationally as a single opening which may vary with time. The reference values of the CEG-LBS are listed in the Table.

CEG-LBS REFERENCE DATA	
DRIVERS	
Reference Volume (7 drivers), V_{ref}	303 m^3
Reference Length (RL), L_{ref}	44 m
Nominal Diameter, D_{drv}	1.33 m
Ratio of Throat-to-Driver Area	1:4
EXPANSION TUBE	
Reference Area, A_{ref}	70.8 m^2
Reference Hydraulic Diameter (DIA), D_{ref}	9.495 m
Test Section Location Measured from Nozzle Exit, X_{sta}	66.5 m
Nominal Expansion-Tube Length, L_{net}	105 m
Ratio of Throat-to-Reference Area	1:29

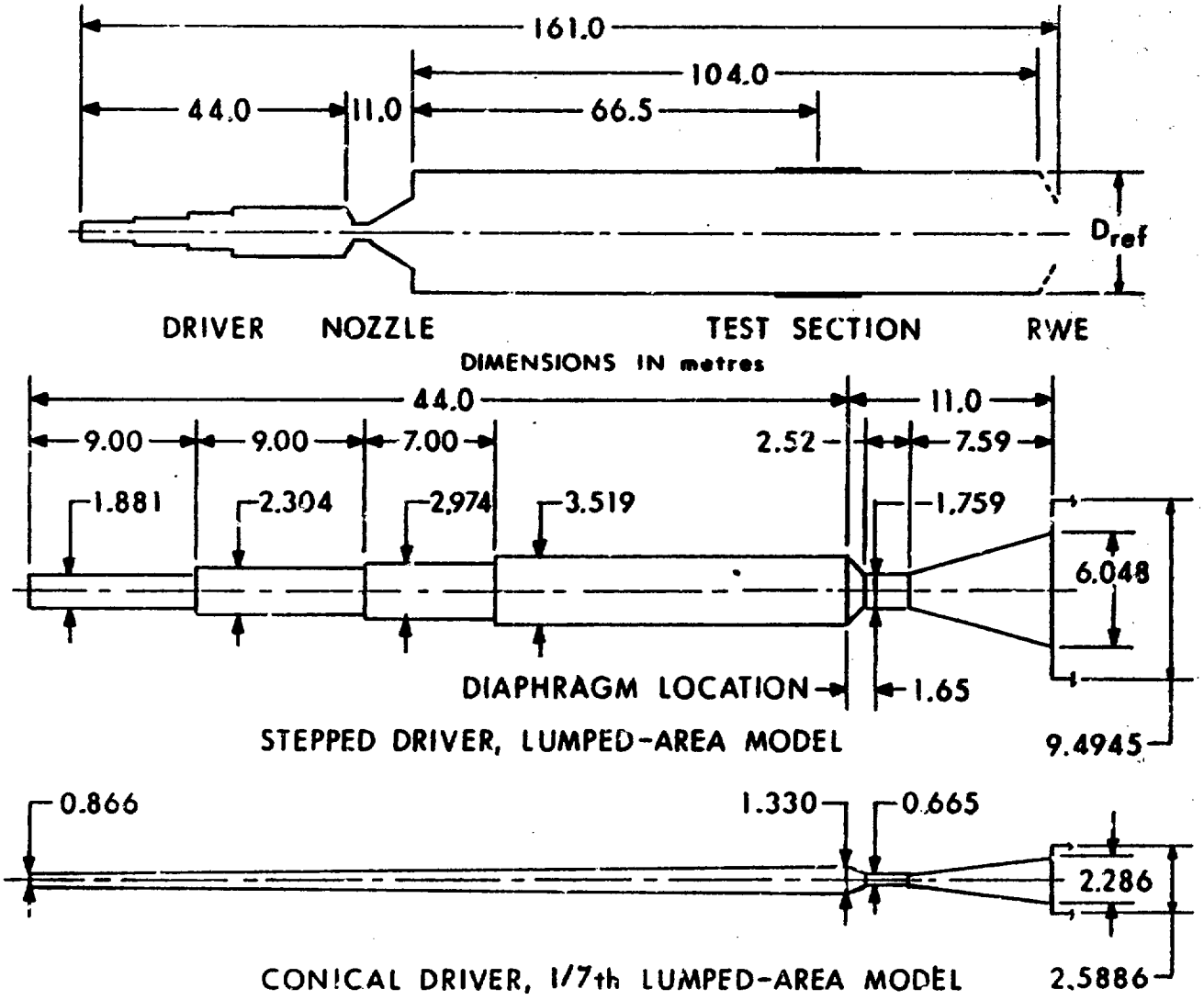

Figure 3: The Computational LBS Model.

[illegible] lumping of the areas changes the cone angles of the convergent and [illegible], the suggestion was made to use a 1/7th lumped-area model in the com[illegible] model, the nozzle sections retain their true angles, the expansion tube has 1/7t[illegible] nal area, and the stepped driver has 1/7th of the 7-driver volume of the LBS [illegible] The 1/7th stepped driver was shaped into a frustrum of a cone by determining the smaller end diameter from 1/7th of the reference driver volume, the reference driver length, and the reference driver diameter of the French LBS. Many comparison calculations of the two driver types were made to ensure that this simplification could be maintained without compromising the results.

Comparisons made to compare the two models described above yielded nearly identical results. The only differences observed are related to the limited accuracy of the input data. Since the RL-Q1D code is one-dimensional, the magnitude of the cross-sectional areas does not alter the results of the flow computations as long as the area ratios remain the same. Any scaling done to extend the operating range of the LBS has to occur in the direction of the flow.

3.2 THE SCOPE OF THE BLAST-WAVE COMPUTATIONS

The design studies were executed for standard atmospheric conditions and based on the use of ambient-temperature air as the driver gas. The blast-wave simulation was related to a scaled, height-of-burst, nuclear explosion of $60m \times W^{1/3}$ by means of an empirical free-field data base. The range of peak overpressures was set from 13.8 to 241 kPa (2 to 35 psi), and the range of weapon yields was set from 1kT to 1MT to include those Army weapon systems which are considered for nuclear hardening. Thus an envelope of test conditions was defined for which a corresponding design envelope of blast-wave simulators of various combinations of driver and expansion-tube lengths had to be found.

As is customary with free-field pressure histories, blast-wave parameters are calculated from the pressure histories of the computationally simulated blast waves. These parameters are compared to those in the empirical data base and thus characterize the simulated blast wave relative to its free-field counterpart. The parameters which suitably describe the pressure history of a blast wave,[6,7] are the shock overpressure (p_{so}, i.e. the peak blast-wave overpressure), the arrival time of the shock (t_s), the static-overpressure impulse (I_{so}) and the positive-phase duration (t_+). The blast wave is further characterized by the dynamic-pressure history. The characteristic parameters of the dynamic-pressure history are the peak dynamic pressure (q), the dynamic-pressure impulse (I_q) and the dynamic-pressure positive-phase duration (t_{+q}).

The shock overpressure is the independent parameter used for accessing the data base of free-field blast-wave parameters. The table values of the static-overpressure impulse and of the dynamic-pressure impulse and their computational counterparts are then used to determine two equivalent weapon yields for the simulated blast-wave from Sachs' scaling laws.[6,7] One weapon yield is based on the impulse of the static overpressure history, while the other weapon yield is based on the impulse of the dynamic-pressure history.

3.3 DRIVER LENGTH

The impulse which an LBS-generated blast wave can deliver is proportional to the mass of the driver gas. The driver gas is held however at such a pressure that a desired shock overpressure will be obtained at the test section located 7 hydraulic diameters downstream from the exit of the divergent nozzle. This condition and the ambient temperature define the density of the driver gas and with the gas parameters fixed, the impulse becomes proportional to the driver volume. The ratios of the cross-sectional areas of the driver assembly are fixed design features. (As we will see in the discussion, changing the proportions of the cross-sectional areas would alter the results.) Therefore, the driver length is the only design parameter which we are

free to change in order to adjust the mass of the driver gas.

To determine the required driver volume and pressure for generating a blast wave of given shock overpressure and weapon yield at the test section, LBS calculations were carried out for a great variety of driver lengths and pressures. Figure 4 shows the results of the driver-length predictions. These curves relate the driver length normalized by the reference driver length of the CEG-LBS (1 RL = 44 metres) to the simulated weapon yield. The results were obtained by monitoring the static and dynamic pressure histories at the test section. The constant-pressure curves in Figure 4 show that the driver length has to be increased in order to increase the weapon yield.

There are two families of curves presented in Figure 4. One family of curves (Figure 4a) relates to the weapon yield calculated from the static-overpressure impulse, and the other one (Figure 4b) relates to the weapon yield calculated from the dynamic pressure impulse. The results of the calculations show that the two yields do not match the equivalent free-field yields; i. e. the two impulses generated in the LBS facility are not related to each other in the same fashion as those generated in a free-field, spherical explosion. Both predictions are important, however, for the loading of targets. Damage due to target crushing occurs in the diffraction phase and is related to the static-overpressure loading, while damage due to overturning and tumbling occurs in the drag phase and is dominated by the dynamic-pressure loading.

The results of this study show that the driver length varies greatly within the given scope of shock overpressures and weapon yields. The variation is greatest when the weapon yield is based on the dynamic-pressure impulse (Figure 4b). The shortest driver required for generating a 240-kPa/2-kT blast wave is only 1 metre long (lower left corner of the graph). The longest driver required for generating a 14-kPa/1-MT blast wave is 5 times the length of the reference driver (upper right corner of graph).

The predictions indicate that for shock overpressures of 170 kPa and above, and high yields, the recompression shock is swept past the test station destroying the blast-wave simulation in the process. This effect appears to be less pronounced when the weapon yield is based on dynamic-pressure impulse; but the pressure histories show that these impulses are distorted by the expanded, low-temperature, high-density driver gas behind the contact surface which passes through the test section prior to the advent of the recompression shock. More will be said about this phenomenon in the next chapter.

3.4 EXPANSION-TUBE LENGTH WITHOUT RWE

The discussion of wave patterns in blast-wave simulators (Section 2.3) mentioned that a rarefaction wave begins to travel upstream after the incident shock has exited the open end of the expansion tube, unless an RWE prevents the formation of such a wave. An alternative method to prevent this rarefaction wave from reaching the test section during the test period and destroying the blast-wave simulation in the process is to make the expansion tube long enough that the rarefaction wave arrives at the test section only after the blast-wave simulation has been completed. The minimal length of such an expansion tube would be the length for which the first expansion wave reaches the test section just at the end of the positive phase of the blast wave. This was the goal of the second study. Its purpose is to aid the project engineer in estimating the trade-off cost of alternative designs.

Figure 5 shows the results of this study. Again, two families of curves are presented. Figure 5a presents the minimum required expansion-tube length versus weapon yield based on static-overpressure impulse. This length was determined by shortening an initially very long tube in consecutive computations, until a length was found for which the positive-phase duration of the simulated blast wave matched the positive-phase duration of the equivalent

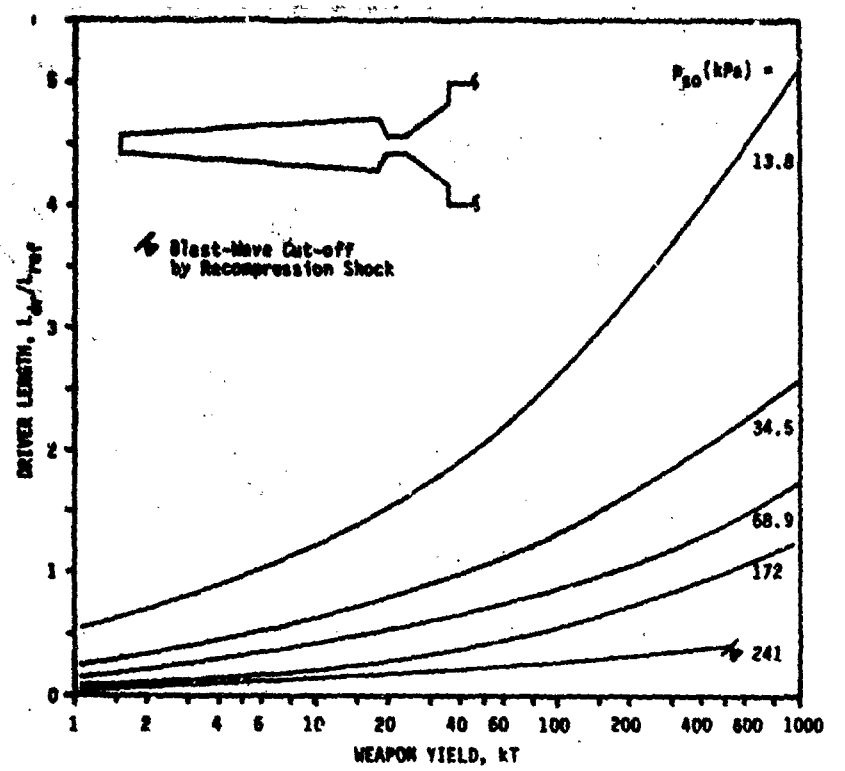

(a) Based on Static-Overpressure Impulse

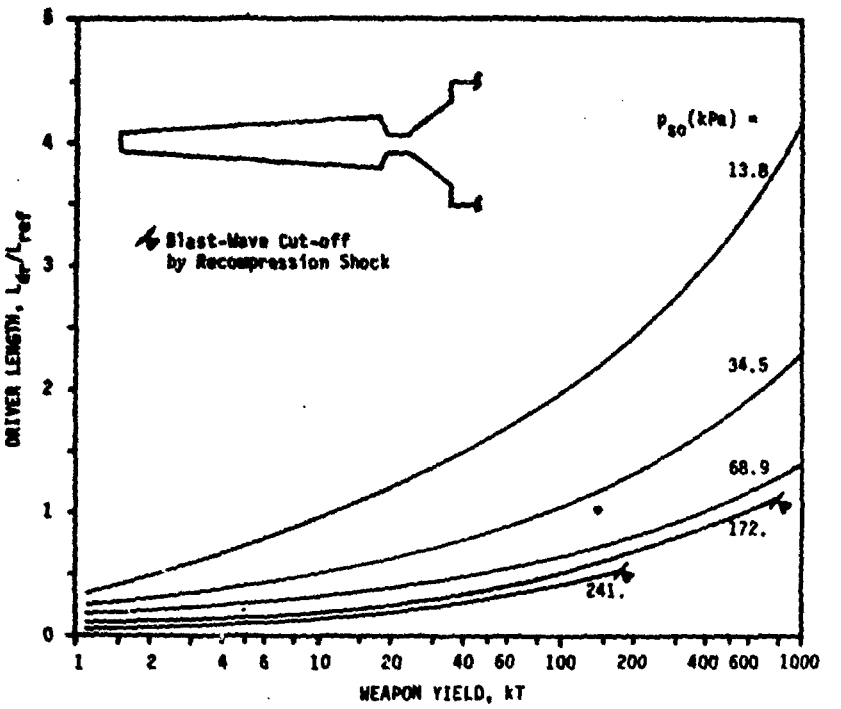

(b) Based on Dynamic-Pressure Impulse

Figure 4: Driver Length Versus Weapon Yield

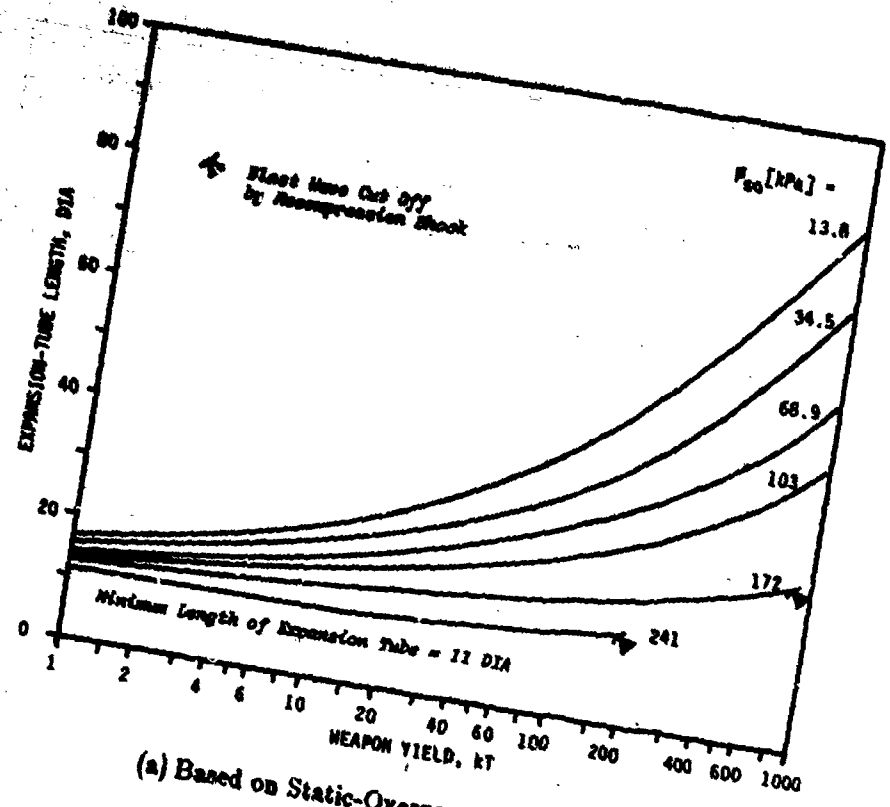

(a) Based on Static-Overpressure Impulse

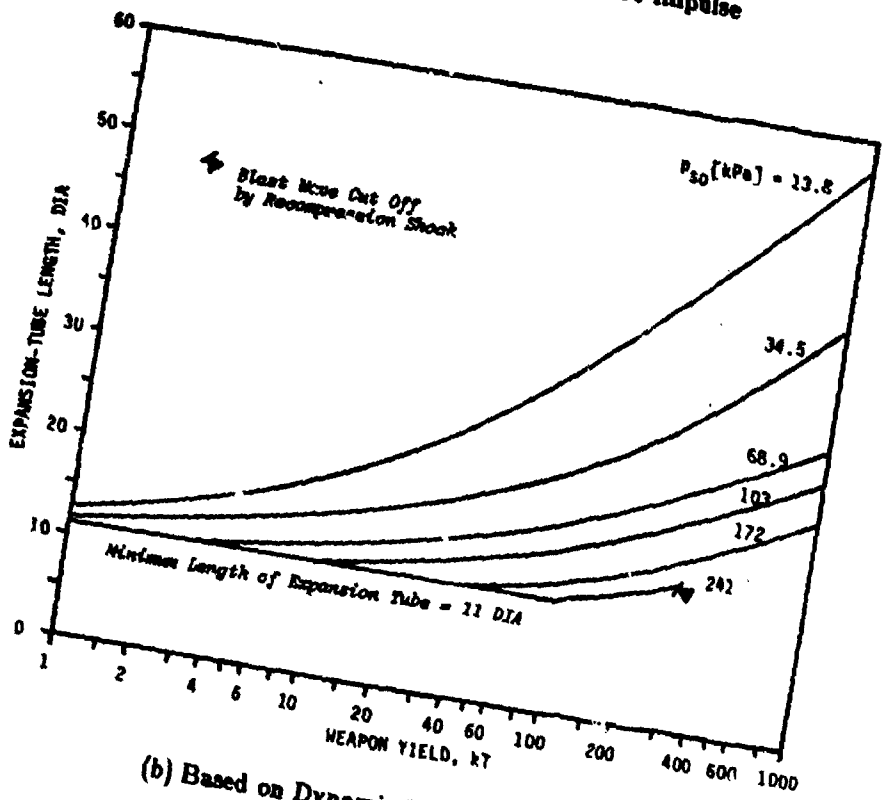

(b) Based on Dynamic-Pressure Impulse

Figure 5: Expansion-Tube Length Without RWE Versus Weapon Yield

free-field blast wave. This could be done only after the driver pressure and the driver length had been determined for each particular blast wave characterized by the shock overpressure and the weapon yield. The longest expansion tube is needed for simulating a 14-kPa/1-MT blast wave; it is 810 metres long (85 D_{ref}'s).

Figure 5b presents the minimum required expansion-tube length versus weapon yield based on dynamic-pressure impulse. We chose to match the free-field, dynamic-pressure impulse in order to obtain somewhat shorter expansion-tube lengths instead of matching the free-field, dynamic-pressure, positive-phase duration which would have lead to even longer expansion tubes than in the static-overpressure case. The expansion-tube length was chosen such that the rarefaction wave from the open end curtailed the positive-phase duration once the dynamic-pressure impulse reached a value greater than 97% of the free-field value. This approach is justifyable because the low dynamic-pressure loads toward the end of the positive phase do not make a noticeable contribution to the overturning of targets, and results in a considerable savings in expansion-tube length as can be learned from a comparison of the results in Figures 5a and 5b. The longest driver measures now 550 metres (57 D_{ref}'s), which represents a length reduction of 32%.

3.5 EXPANSION-TUBE LENGTH WITH PASSIVE RWE

A further reduction of the expansion-tube length is anticipated from the utilization of a passive RWE at the open end of the tube. A passive RWE is initially set to an open-area ratio which remains fixed throughout the test. The study is complicated, therefore, by the presence of this second, unknown quantity, which must be set such that neither a rarefaction wave nor a shock will be generated, and travel upstream. The critical value of this quantity must be known before the minimum length of the expansion tube with passive RWE can be determined. For a first guess, a steady-state, one-dimensional analytical solution of the inviscid flow of an ideal gas through a converging nozzle was used[8] to determine the critical area ratio for which the throat Mach number at the tube exit will equal the isentropic discharge Mach number of the flow behind the incident shock. This analytical solution is shown in Figure 6 as a dashed line.

Although the analytical solution in Figure 6 does not match the experimental RWE settings which were used in blast-wave simulations at the CEG,[9] it affords a starting point for the present investigation. Together with the experimental values, the analytical solution indicates in which direction the search for the critical value should continue. Beginning therefore with the analytical value for the RWE open-area ratio, we proceeded to determine this ratio for given driver conditions with a matrix of test conditions in which two parameters, i.e. the RWE open-area ratio and the tube length, were systematically changed until the static-overpressure impulse and the positive-phase duration of the simulated blast wave both matched the corresponding parameters of the equivalent free-field blast wave. This was done for selected shock overpressures ranging from 14 to 240 kPa and the results are shown in Figure 6 as a solid line.

Once the RWE open-area ratio was determined as a function of the shock strength, P_2/P_1, computations could then be performed for various weapon yields by changing the driver length at constant driver pressure (defining the desired shock overpressure). The minimum required length of the expansion tube was determined by shortening a long tube in consecutive computations until the free-field criterion was met. Figure 7 presents the results of this study. As before, two families of curves are shown, one for the weapon yield based on static-overpressure impulse (Figure 7a), the other for the weapon yield based on dynamic-pressure impulse (Figure 7b). As in the preceding study, the free-field criterion for the data in Figure 7a was the positive-phase duration, and the free-field criterion for the data in Figure 7b was the 97% mark of the dynamic-pressure impulse. The results show that the length of the expansion tube with passive RWE for a 14-kpa/1-MT blast wave is still 510 metres (54 D_{ref}'s) and

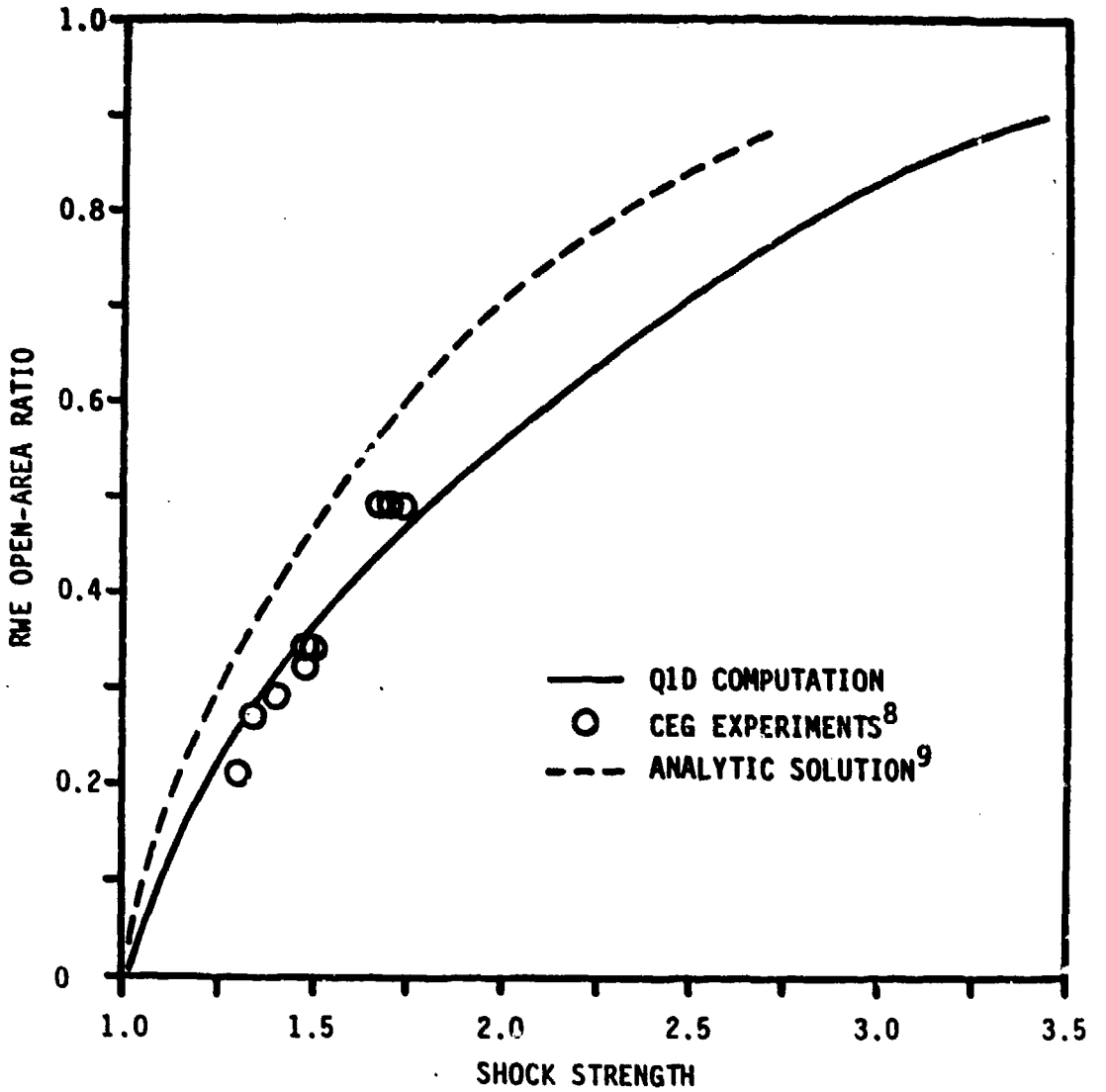

Figure 6: RWE Open-Area Ratio Versus Shock Strength

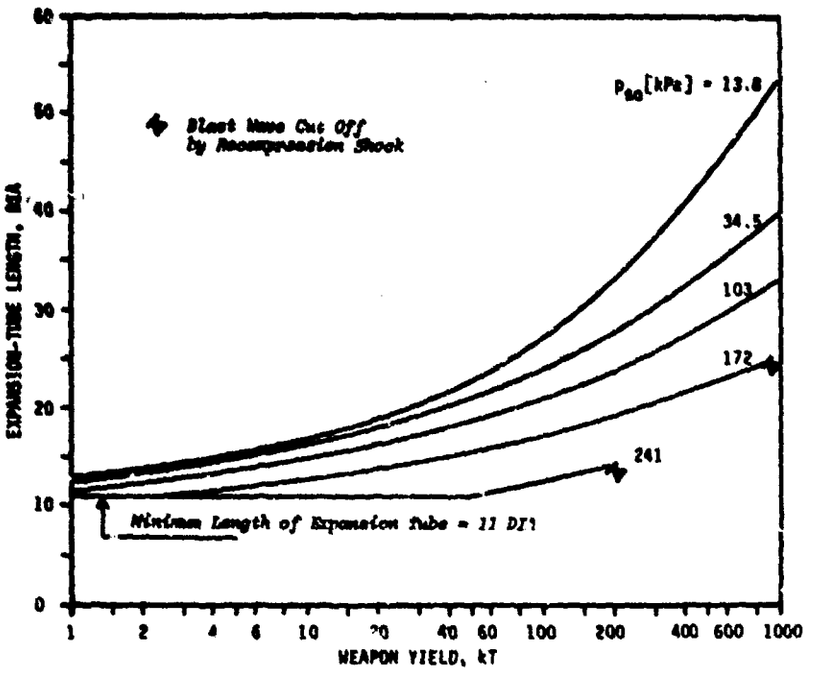

(a) Based on Static-Overpressure Impulse

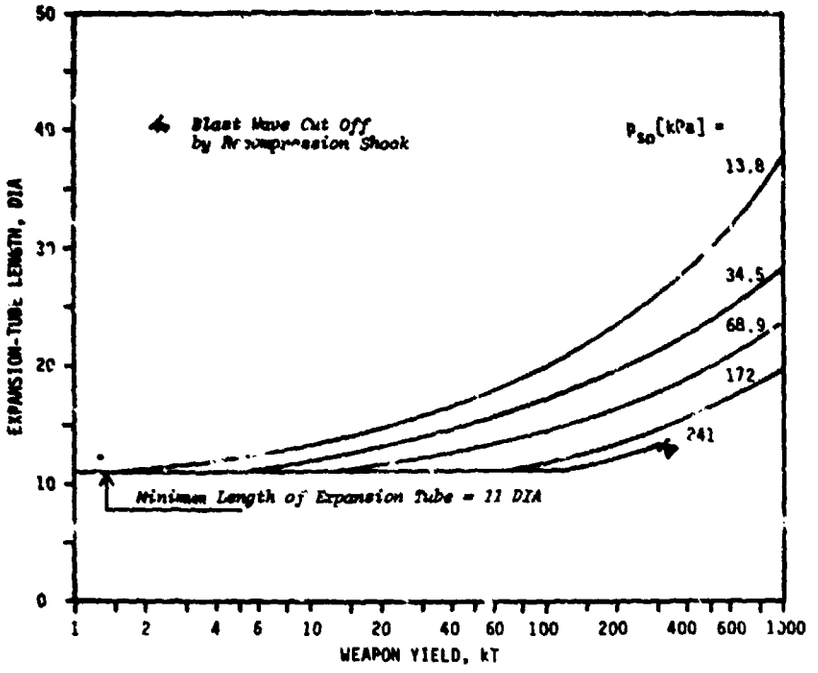

(b) Based on Dynamic-Pressure Impulse

Figure 7: Expansion-Tube Length With Passive RWE Versus Weapon Yield

360 metres (38 D_{ref}'s), respectively depending on whether the yield is based on static-overpressure, or dynamic-pressure impulse.

3.6 DESIGN ENVELOPES

From the results of our numerical studies, design envelopes can be defined for any LBS facility with the same cross section as the CEG-LBS. This was done in Figures 8 and 9 in graphs of blast-wave peak overpressure versus weapon yield. (The peak overpressure of the blast wave is the shock overpressure.) Figure 8 presents the design envelopes for an LBS without RWE, and Figure 9 presents the design envelopes for an LBS with passive RWE. Two design envelopes are shown in each figure, one for weapon yields based on static-overpressure impulse, and another for weapon yields based on dynamic-pressure impulse. Curves of constant driver length are plotted in multiples of the CEG reference driver length (i.e. 1 RL = 44 metres). Curves of constant expansion-tube length are plotted in multiples of the CEG reference hydraulic diameter (i.e. 1 DIA = 9.495 metres).

The graphs show the driver and expansion-tube lengths needed to simulate a blast wave of given shock overpressure and weapon yield anywhere in the test envelope. Conversely, the graphs will yield the blast-wave conditions (i.e., the peak static overpressure and the weapon yield), which may be simulated by an LBS of given driver, and expansion-tube lengths. The main difference between graphs (a) and (b) is the spread of the driver and expansion-tube lengths required to simulate the blast wave conditions covered by the envelope. The upper left corner and the lower right corner of these graphs present critical design areas. It will be difficult to simulate the high overpressure and low-yield, as well as the low overpressure and high-yield blast wave conditions because of the extreme driver dimensions required.

Comparing the data presented in parts (a) and (b), resp. of Figures 8 and 9 reveals the differences in the LBS design with regard to the test criteria employed. The static overpressure history and its impulse are associated with the diffraction loading of targets. The dynamic pressure history and its impulse are associated with the drag loading and overturning of targets. Most mobile Army systems are more susceptible to damage by overturning and tumbling than to damage by diffraction loading. Therefore, it is necessary to use the overturning criterion in the design of an LBS. The comparison reveals that somewhat longer drivers are needed when the weapon yield is based on the dynamic-pressure impulse. At the same time, the expansion tubes are considerably shorter. This result was achieved by using a less restrictive matching criterion than t_{+q}, i.e. the 97%-mark of I_q, thereby cutting off the tail of the dynamic-pressure history. Otherwise, the lengths of the expansion tube would have been longer, also. The savings in expansion-tube length are on the order of 30% without and with passive RWE, measured at the 14 kPa/1 MT point.

The effect of a passive RWE on the design of an US-LBS can be studied by comparing Figures 8b and 9b, and Figures 8a and 9a, respectively. There is no difference in driver-length requirements in this comparison. The LBS-design differences with regard to the passive RWE installed at the open end of the expansion tube basically amount to savings in length. The comparison shows that in both cases, (a) based on I_{so} (diffraction loading) and (b) based on I_q (drag loading), the RWE effects a 40% savings in the length of the expansion tube, measured at the 14 kPa/1 MT point. A passive RWE will be employed if this savings translates into saved dollars over and above the construction cost of a passive RWE. An active RWE with programmed, adjustable open area should be employed for wave shaping if the construction cost for the longest expansion tube without RWE, as well as the combined cost of expansion tube and passive RWE both exceed the construction cost of the active RWE system.

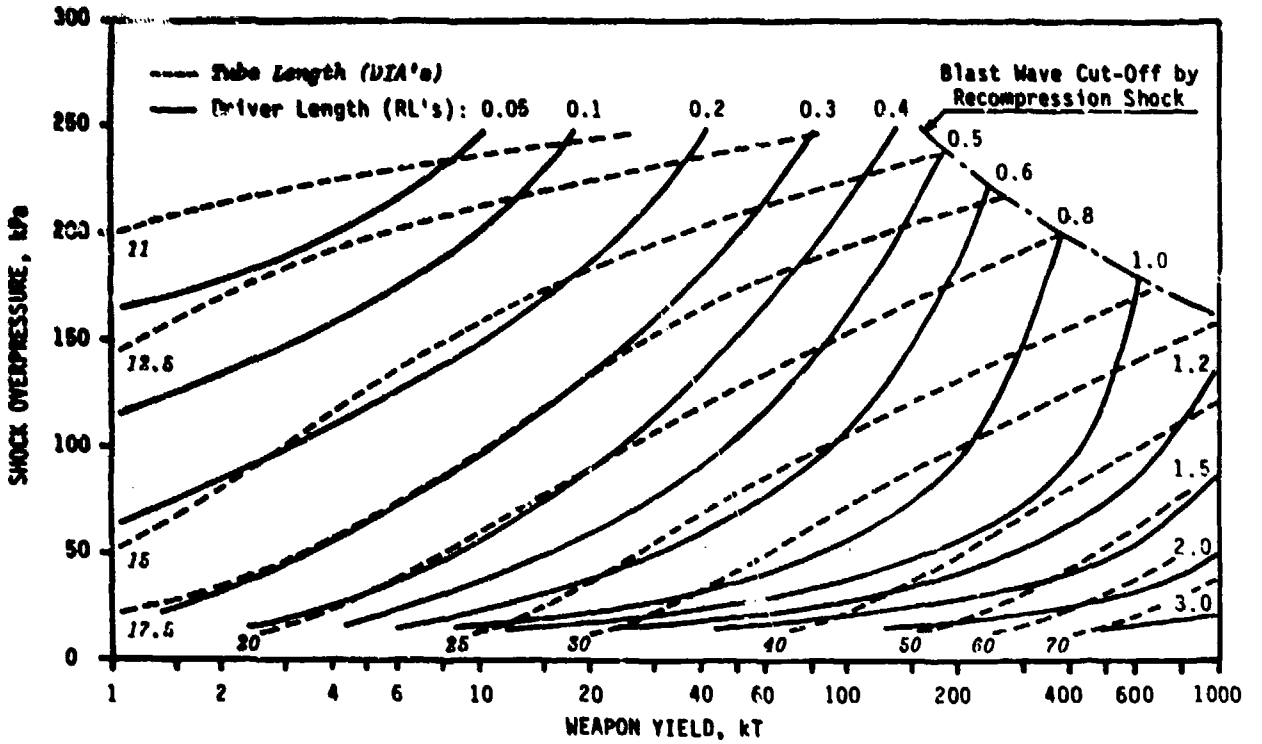

(a) Based on Static-Overpressure Impulse

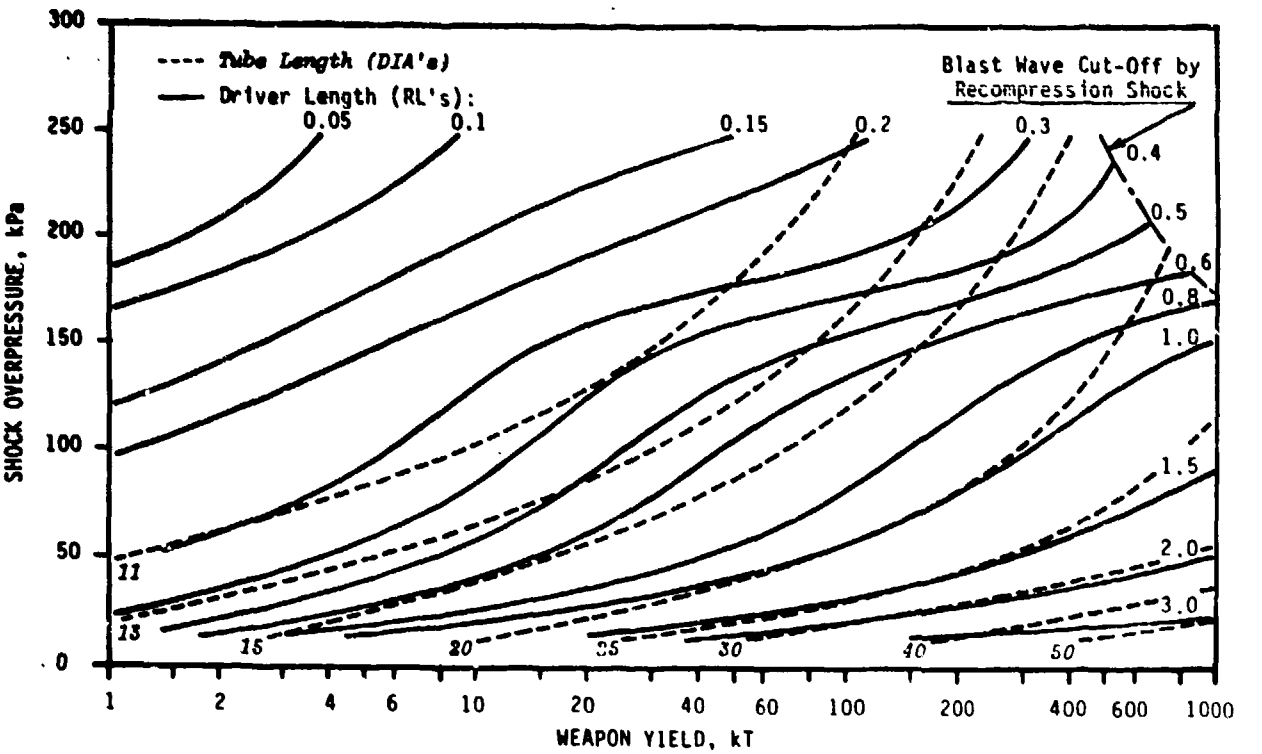

(b) Based on Dynamic-Pressure Impulse

Figure 8: Design Envelopes for a US-LBS Without RWE

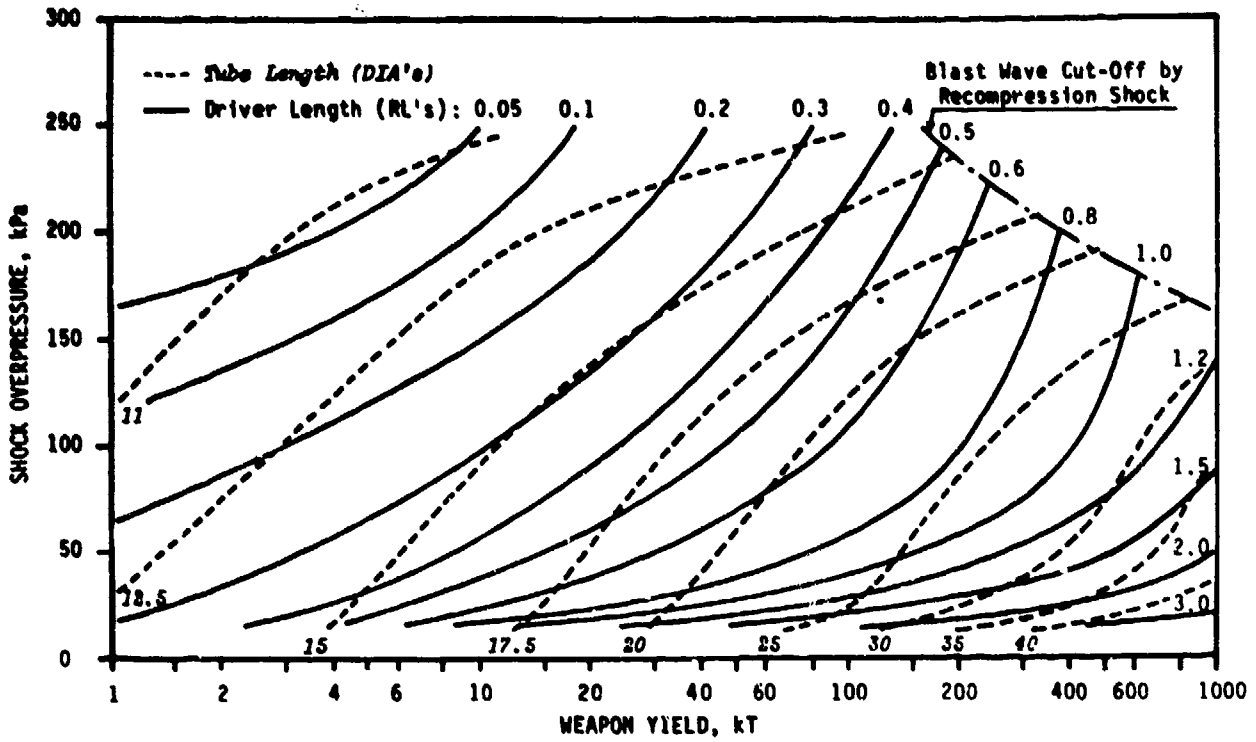

(a) Based on Static-Overpressure Impulse

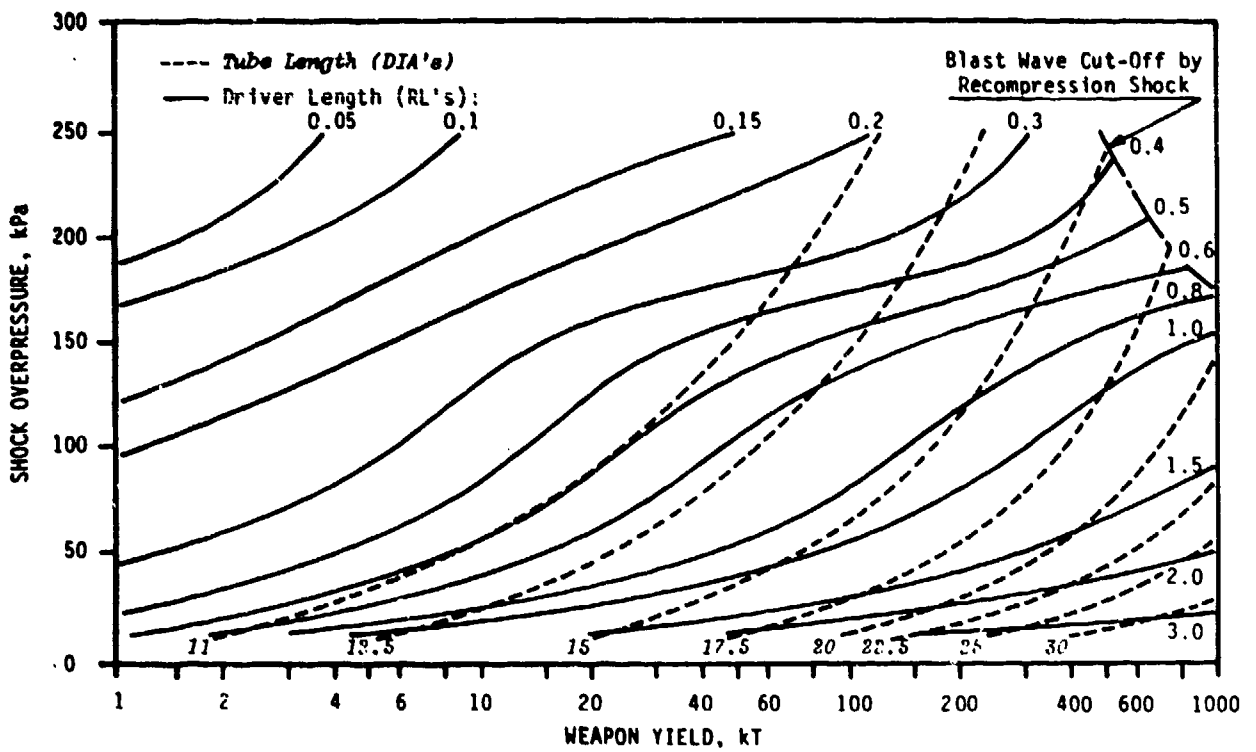

(b) Based on Dynamic-Pressure Impulse

Figure 9: Design Envelopes for a US-LBS With Passive RWE

4. DISCUSSION OF THE RESULTS

The parametric studies are showing that the driver length is a critical design parameter because extreme dimensions are required to cover the entire design envelope. For blast-wave simulators using unheated driver gas, the driver pressure is a critical design parameter, also. Furthermore, the volume distribution in the driver assembly influences the resulting simulation. Finally, the location of the test section is critical because of the movement of the recompression shock and the contact surface.

4.1 DRIVER-DESIGN CONSIDERATIONS

Very short drivers and very high driver pressures are required to simulate the high shock overpressure/low yield blast waves represented by the upper left corners of the design envelopes shown in Figures 8 and 9. Figure 10 presents the shock overpressure obtained computationally as a function of the driver pressure. The inviscid, ideal-gas Q1D computations were done for the reference driver length and two nozzle configurations. The graph shows that a driver pressure of 110 atm is required to produce a 172-kPa blast wave at the test section. The driver pressure increases to 190 atm for producing a 240-kPa blast wave at the test section. Experiments carried out in a blast-wave simulator model here at the BRL[10] indicate that real-gas effects become significant at driver pressures above 150 atm. Therefore, the experimentally required pressures are expected to be even higher than the computational values. While it may be possible to engineer these drivers, building them would be very expensive.

Figure 11 illustrates still another physical flow phenomenon that requires a further increase in driver pressure. As mentioned above, the driver volumes required to simulate low-yield blast waves at high shock overpressures are very small. Since the cross-sectional areas are inalterable quantities, the only way in which the volume can be reduced is by shortening the driver length. The shorter the driver, however, the sooner will the rarefaction waves reflected from the driver-end wall catch up with, and overtake, the incident shock thereby diminishing its strength. The data in Figure 11 show that the increase in driver pressure, necessary to compensate for this effect can be considerable. The question may arise in the mind of the reader that heating the driver gas might solve this problem, and we will address this question at the end of our discussion.

Very long drivers are required for simulating low shock-overpressure/high-yield blast waves. Computations were carried out for two conical drivers with different cone half-angles because computations for a cylindrical driver[11] yielded results which were inconsistent with the results of this study. The results of these computations show the influence of the driver shape on the simulated blast wave. They are presented in Figure 12, where the driver volume is plotted versus weapon yield for three shock-overpressure levels. The effect of the driver shape on the blast wave is most pronounced at the 14-kPa shock-overpressure level and becomes negligible at the 69-kPa shock-overpressure level. The results indicate that (1) a cylindrical driver requires less volume to produce a blast wave of stated shock overpressure and weapon yield, (2) the significant parameter in our Q1D computational study is the driver length, and (3) wave-shaping has to be paid for with extra volume added to the driver design.

4.2 TEST-SECTION LOCATION

For economic reasons, the test section should be located as close as possible to the exit of the multiple-driver nozzles in order to keep the expansion tube short. Six reference diameters of the expansion tube are considered the necessary length for proper mixing of the flow from the multiple drivers. Therefore, the test section must be located more than six reference diameters

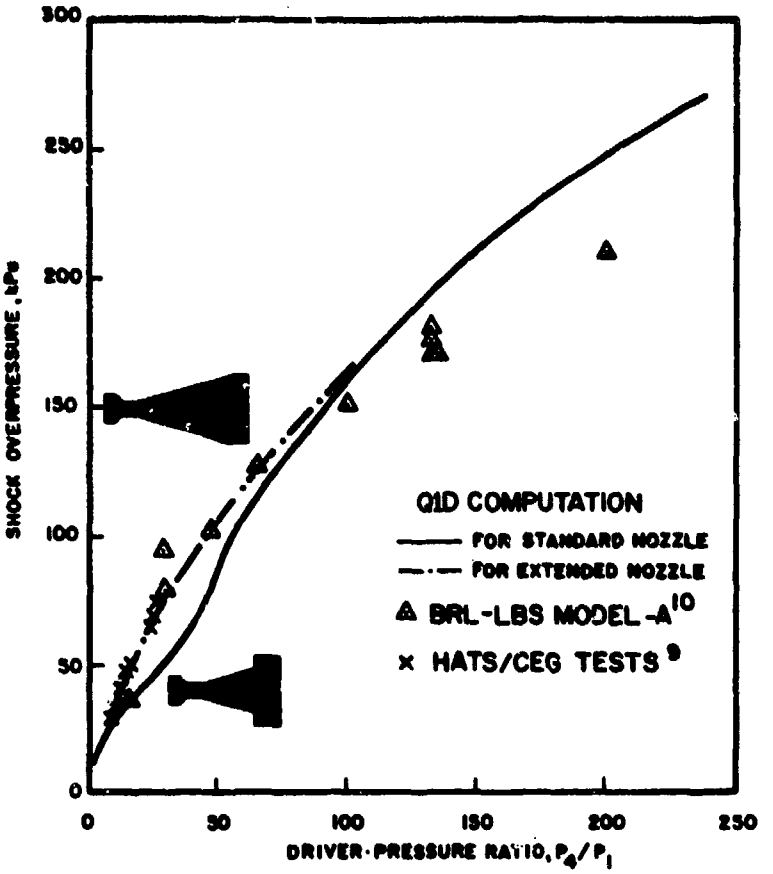

Figure 10: Computational Shock Overpressure Versus Driver Pressure

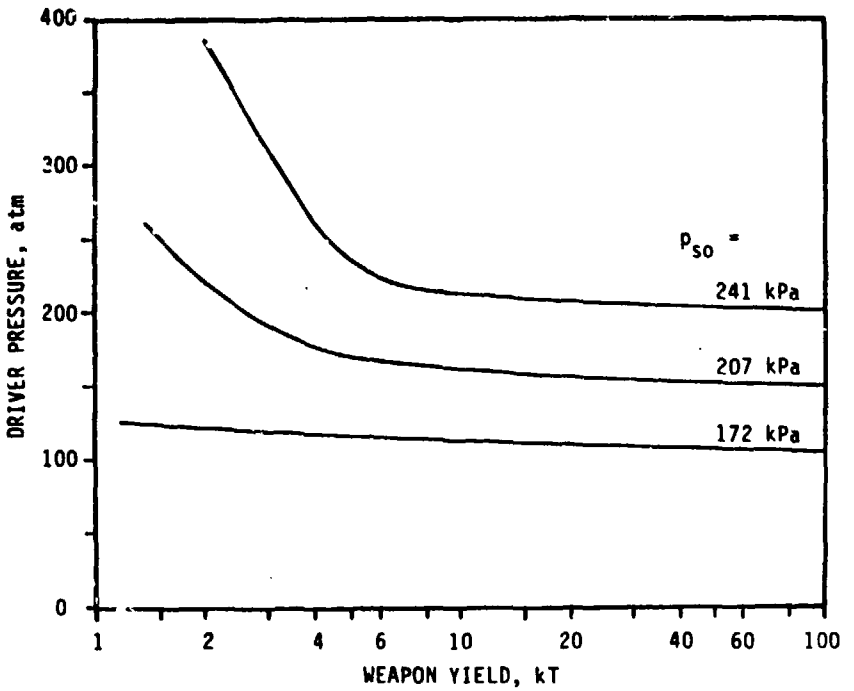

Figure 11: Driver Pressure as a Function of Weapon Yield for Constant Shock Overpressure at the Test Section

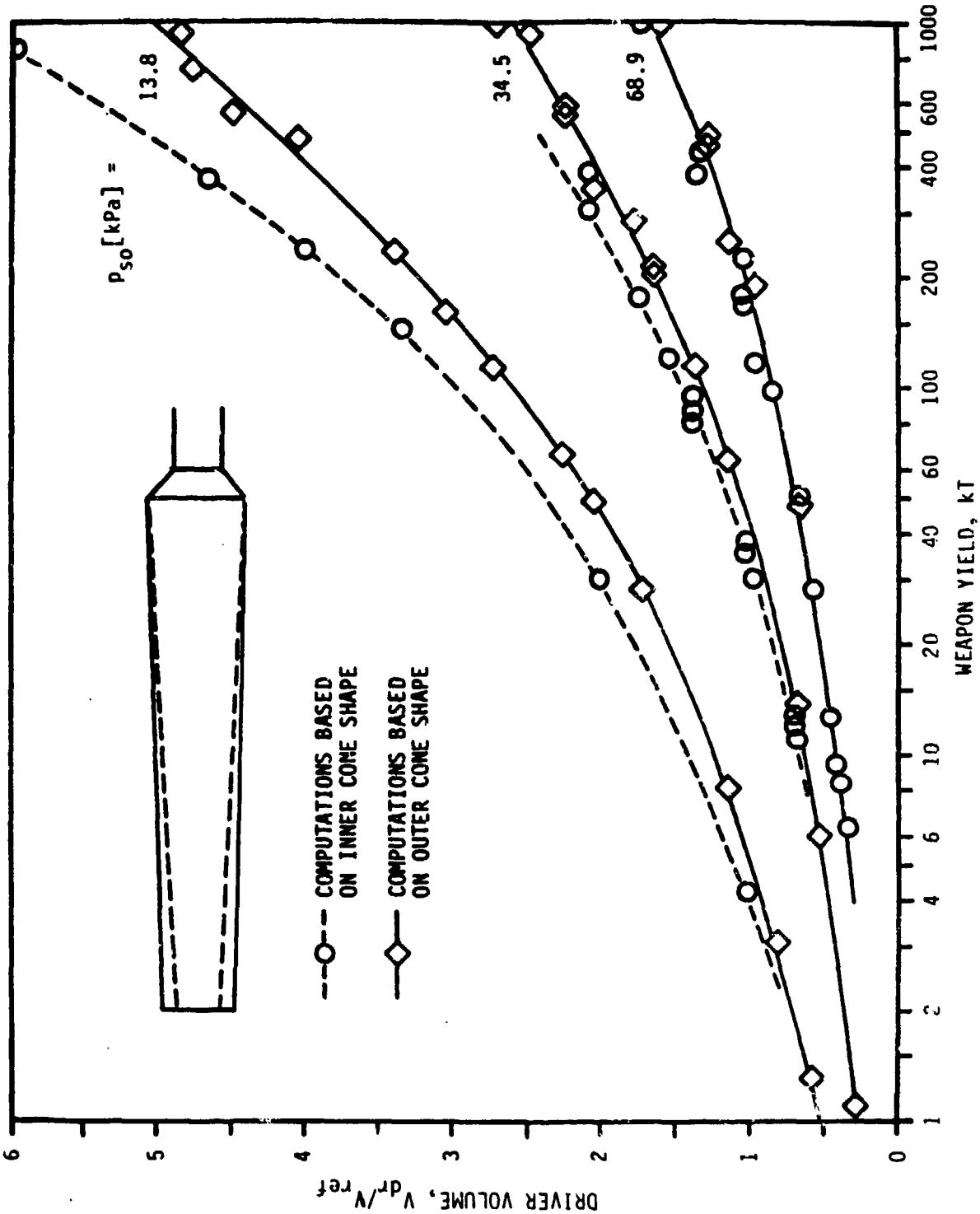

Figure 12: Influence of Driver-Cone Shape on Weapon Yield.

downstream from the exit of the nozzles. For blast-wave simulators using unheated driver gas, the movement of the contact surface and of the recompression shock have an important impact on the location of the test section because the passage of either wave through the test section during the positive phase destroys the simulation.

The effects of the passage of the recompression shock and of the contact surface through the test section are illustrated in Figure 13. The pressure histories represent the computational simulation of a blast wave of high weapon yield with a shock overpressure of 241 kPa (35 psi). In Figure 13a, the static and dynamic pressure histories were recorded at seven hydraulic diameters from the exit of the divergent nozzles. The first jump in dynamic pressure at 0.35 sec is due to the arrival of the cold driver gas behind the contact surface. The large drop in static pressure and the associated increase in dynamic pressure at 0.60 sec is due to the arrival of the recompression shock.

The passage of the recompression shock can be avoided by moving the test station farther from the drivers. Figure 13b shows the pressure histories from the same calculation recorded at twelve diameters downstream from the beginning of the expansion tube. The recompression shock does not pass through this station, but the effects of the passage of the contact surface can still be recognized in the bulging of the dynamic-pressure curve.

The jump in dynamic pressure across the contact surface is caused by the cooling of the expanding driver gas. The effect is particularly strong in those flow situations in which the recompression shock leaves the divergent nozzle ($p_{ss} > 70\ kPa$). To avoid the undercooled driver gas behind the contact surface, the test section will have to be relocated far downstream to where the contact surface will not arrive before the end of the positive-phase duration. For shock overpressures of 70 kPa and less, the density mismatch across the contact surface is insignificant, and the test section can be maintained at the present location.

The movements of the recompression shock and of the contact surface were studied for various shock overpressures, and the results of this study are presented in Figure 14. The maximum distance which the recompression shock moves from the exit of the nozzle is given in Figure 14a as a function of the simulated yield. Curves are given for three shock overpressures, 243, 210 and 174 kPa (i.e. 35, 30 and 25 psi). For each shock overpressure, the simulated yield shown is calculated from the static-overpressure impulse. The curves indicate that the recompression shock will pass through the test section, located at seven hydraulic diameters (66.5 m) from the exit of the nozzle, for blast waves with peak overpressures in excess of 175 kPa and high yields.

Figure 14b shows the maximum distance which the contact surface travels from the exit of the nozzle, as a function of the simulated weapon yield. Curves are given for three shock overpressures, 243, 174 and 105 kPa (i.e. 35, 25 and 15 psi). For each shock overpressure, the simulated weapon yield was calculated from the dynamic-pressure impulse. The curves show that for the extreme case of a 240-kPa/1-MT blast wave the test section would have to be moved from 66.5 to 360 metres downstream from the exit of the nozzle adding considerable length to the expansion tube. Studying the effects of heating of the driver gas on the test conditions of blast-wave simulators is therefore of great importance.

4.3 DRIVER-GAS HEATING

The high driver pressures required to generate the desired shock overpressures in the design envelope of the LBS, and the mismatched densities at the contact surfave due to the cold, expanded driver gas are compelling factors in the search for a better solution to the blast-wave-simulation requirements as posed by the US Army. Heating the driver gas to an appropriate level would allow matching the density across the contact surface, thereby

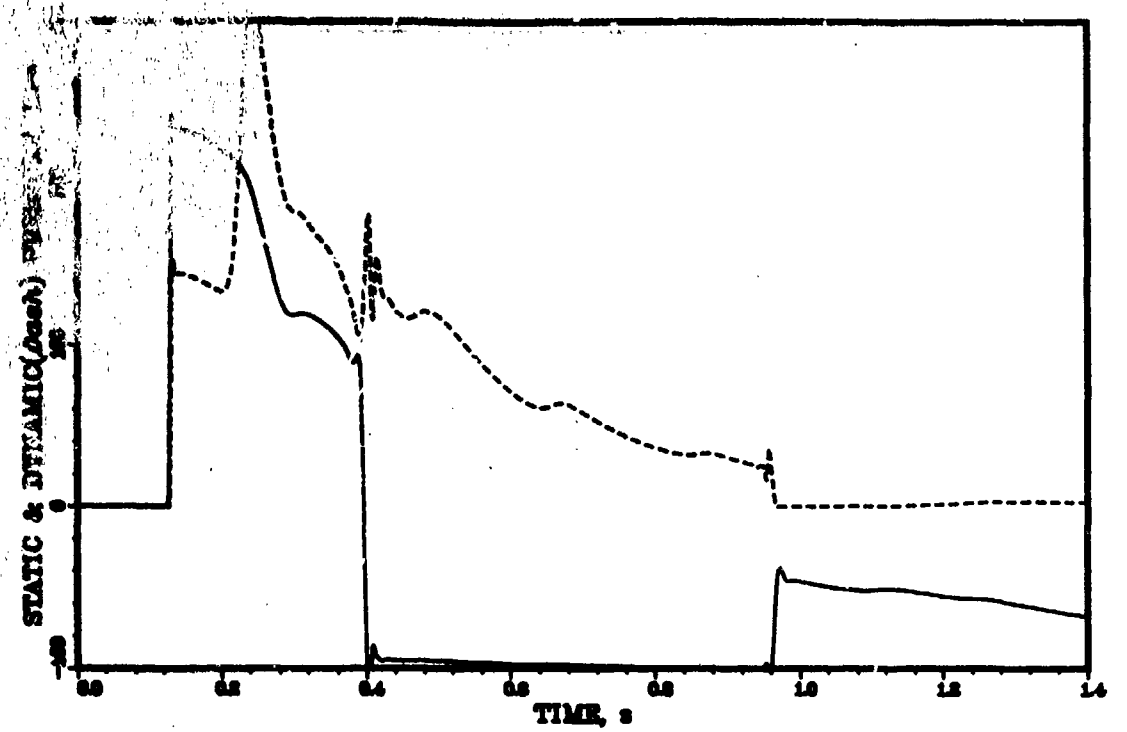

(a) Passing of the Recompression Shock at the 7-DIA Test Section

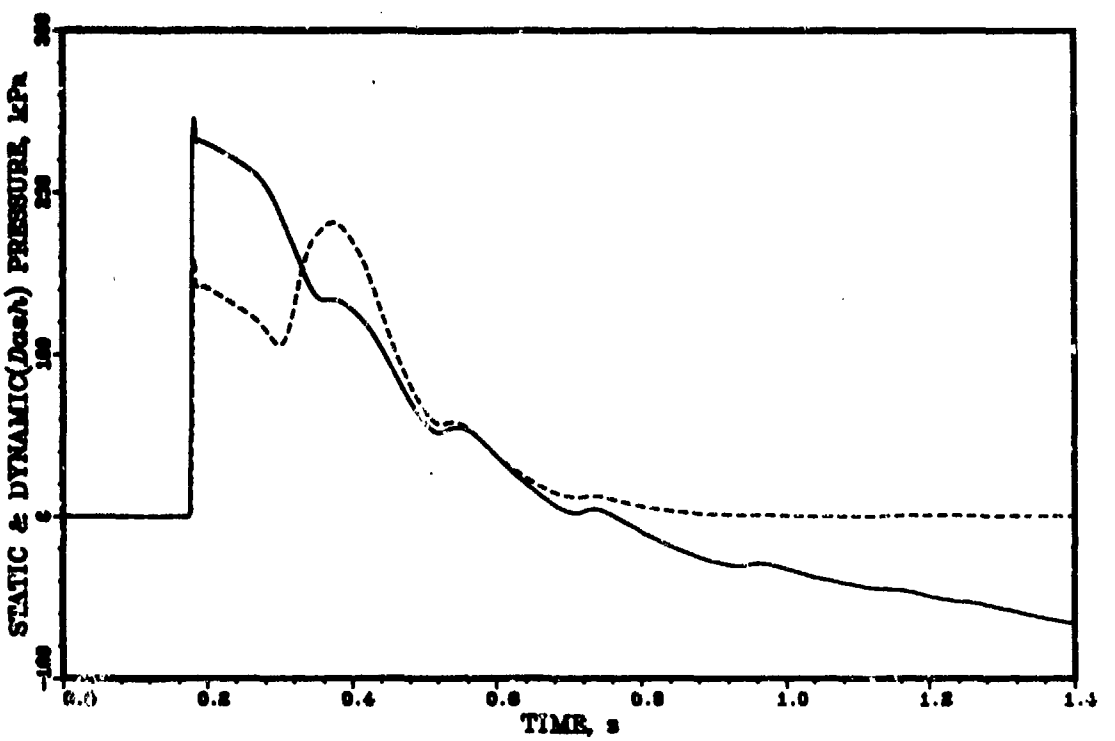

(b) Passing of the Contact Surface at the 12-DIA Test Section

Figure 13: Effects of Recompression Shock and Contact Surface on the Pressure History of a Simulated Blast Wave.

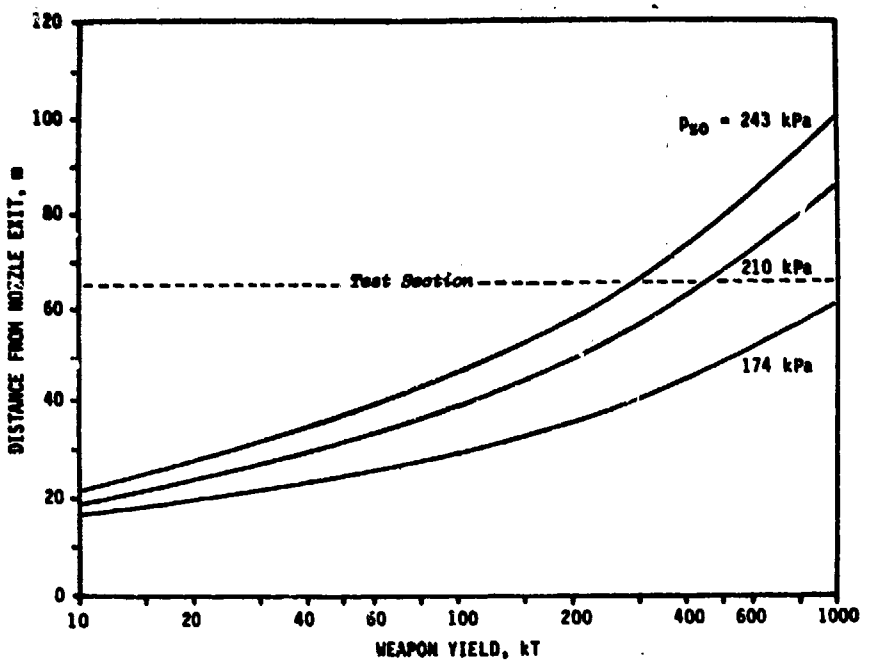

(a) Extreme Position of the Recompression Shock

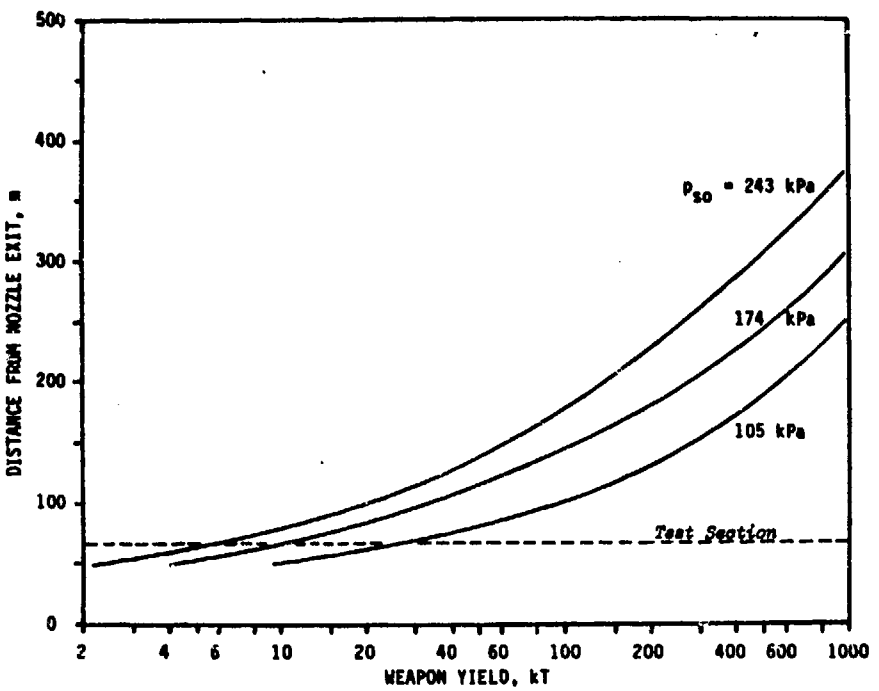

(b) Extreme Position of the Contact Surface

Figure 14: Movement of Recompression Shock and Contact Surface Versus Weapon Yield at Constant Shock Overpressure.

eliminating the need for moving the test section farther downstream from the present position, which is 66.5 metres from the nozzle exit.

Computational studies were carried out at the BRL by this and other authors and reported at the 9th International Symposium on Military Applications of Blast Simulation.[11] The results of these studies can be summarized as follows.

(a) By heating the driver gas, the maximum driver pressure can be kept below the limit imposed by material stress criteria. For practical reasons of the LBS-design, this limit was chosen at 120 atm.

(b) Heating the driver gas requires larger driver volumes particularly at the high-shock-overpressure/low-yield end of the design envelope, where the extremely short driver lengths with cold driver gas pose a problem.

(c) Heating makes possible the matching of the density across the contact surface, and eliminates the need to relocate the test section farther downstream from the exit of the nozzle.

5. CONCLUSIONS

The present computational LBS studies define operating envelopes for a US-LBS design based on the LBS at the CEG in France. They permit a prediction of the dimensions in length required for operating the LBS over a wide range of shock overpressures and weapon yields. A bigger or smaller LBS can be defined by increasing or decreasing the cross-sectional reference area. However, the results are limited in their applicability to a US-LBS design that preserves the cross-sectional area ratios of the French design. The results are particularly sensitive to a change in the throat-area ratio, A_{thr}/A_{ref}. The lengthwise dimensions are not involved in this scaling process.

The results of our studies may be summarized as follows.

(a) The lengths of the driver assembly and of the expansion tube increase with the weapon yield.

(b) For constant yield, the driver pressure increases in proportion to the desired shock overpressure. A 240 kPa blast wave at the test section requires a driver pressure of 200 atm (!); however, for very short drivers, this requirement may increase to twice this value.

(c) The length of the driver assembly based on the drag-loading and overturning criterion, has to be varied from 2 to 220 metres to cover the entire design envelope of the US-LBS.

(d) The length of the driver assembly decreases with increasing shock overpressure. The shortest drivers are required for low-yield blast waves at the 240 kPa (35 psi) shock-overpressure level.

(e) The longest drivers are required for simulating high-yield blast waves at the lower shock-overpressure boundary of of the design envelope. A driver length of 220 metres is required at the 14 kPa/1 MT point.

(f) Basing the LBS dimensions on the dynamic-pressure impulse (i.e. the overturning criterion) rather than the static overpressure impulse necessitates somewhat longer drivers and affords shorter expansion tubes.

(g) The longest expansion tube simulating the entire positive phase of a 14 kPa/1 MT blast wave measures 783 metres without RWE and 513 metres with passive RWE for a test section located at 66.5 metres from the exit of the divergent nozzles.

(h) The passive RWE saves up to 40% of expansion-tube length with the test section located at 66.5 metres from the end of the divergent nozzles.

(i) The test section has to be moved downstream from its present position as much as 310 metres in order to avoid the undercooled driver gas behind the contact surface at shock overpressures above 69 kPa (10 psi).

Finally, a caution has to be added concerning the one-dimensionality of our approach. The Q1D model should not be expected to accurately simulate the real, three-dimensional flow phenomena occurring in a multiple-driver LBS. Our experimental evidence indicates for instance that the recompression shock is not as strong and does not travel as far downstream as the Q1D computations want to make us believe. Also, the BRL experiments shown in Figure 10 indicate that higher driver pressures than those predicted by the Q1D-computations will be required to obtain shock overpressures above 140 kPa (20 psi).

REFERENCES

[1] Gratias, S. and Monsac, J. B. G., "The Large-Scale Nuclear-Blast Simulator of the Gramat Research Center: (1) Concept, Research, Performance;
(2) Description and Operational Utilisation."
Centre d'Etudes de Gramat, France; in Proceedings of the Seventh International Symposium on the Military Application of Blast Simulation, Medicine Hat, Alberta, Canada, 13-17 July 1981.

[2] Ethridge, N. H., et al., "Computational and Experimental Studies of Blockage Effects in a Blast Simulator", US Army Armament Research and Development Center, Ballistic Research Laboratory, Aberdeen Proving Ground, Maryland, June 1984

[3] Beam, R. M. and Warming, R. F., "An Implicit Factored Scheme for the Compressible Navier-Stokes Equations," AIAA Journal, Vol. 16, No. 4, April 1978, pp. 393-402.

[4] Opalka, K. O. and Mark, A., "The BRL-Q1D Code: A Tool for the Numerical Simulation of Flows in Shock Tubes with Variable Cross-Sectional Areas," BRL-TR, US Army Ballistic Research Laboratory, Aberdeen Proving Ground, Maryland 21005, October 1986.

[5] Mark, A., Opalka, K. O., et al., "Simulation of Nuclear Blasts with Large-Scale Shock Tubes," Ballistic Research Laboratory, Aberdeen Proving Ground, Maryland, USA; in Proceedings of the Eighth International Symposium on Military Applications of Blast Simulation, Spiez, Switzerland, 20-24 June 1983.

[6] Glasstone, S. and Dolan, P. J., "The Effects of Nuclear Weapons", DA-Pamphlet No. 50-3, Headquarters, Department of the Army, Washington, DC, March 1977

[7] Baker, W. E., ed. "Explosions in Air: Engineering Design Handbook, Part One," AMC Pamphlet No. 706-181, Headquarters, U. S. Army Material Command, Alexandria, VA, July 1974

[8] Pearson, R. J., Private Communication, U. S. Army Ballistic Research Laboratory, Aberdeen Proving Ground, Maryland 21005-5066

[9] Tels, G. D., Private Communication, U. S. Army Ballistic Research Laboratory, Aberdeen Proving Ground, Maryland 21005-5066

[10] Hisley, D. M., Gion E. J. and Bertrand, B. P., "Performance and Predictions for a Large Blast Simulator Model," BRL-TR-2647, U. S. Army Ballistic Research Laboratory, Aberdeen Proving Ground, Maryland 21005-5066, April 1985

[11] Pearson, R. J., Opalka, K. O. and Hisley D. M., "Design Studies of Drivers for the US Large Blast/Thermal Simulator," Ballistic Research Laboratory, Aberdeen Proving Ground, Maryland, USA; in Proceedings of the Ninth International Symposium on Military Applications of Blast Simulation, Atomic Weapons Research Establishment Foulness, Southend-on-Sea, Essex, England SS3 9XE, September 1985

DISTRIBUTION LIST

No. of Copies	Organization
12	Administrator Defense Technical Info Center ATTN: DTIC-DDA Cameron Station Alexandria, VA 22304-6145
1	Director of Defense Research & Engineering ATTN: DD/TWP Washington, DC 20301
1	Asst. to the Secretary of Defense (Atomic Energy) ATTN: Document Control Washington, DC 20301
1	Director Defense Advanced Research Projects Agency ATTN: Tech Lib 1400 Wilson Boulevard Arlington, VA 22209
2	Director Federal Emergency Management Agency ATTN: D. A. Bettge Technical Library Washington, DC 20472
1	Director Defense Intelligence Agency ATTN: DT-2/Wpns & Sys Div Washington, DC 20301
1	Director National Security Agency ATTN: E. F. Butala, R15 Ft. George G. Meade, MD 20755
1	Director Joint Strategic Target Planning Staff JCS Offut AFB Omaha, NB 68113
1	Director Defense Communications Agency ATTN: 930 Washington, DC 20305
9	Director Defense Nuclear Agency ATTN: DDST TIPL/Tech Lib SPSS/K. Goering SPTD/T. Kennedy SPAS/P.R. Rohr G. Ullrich STSP/COL Kovel NATD NATA Washington, DC 20305
2	Commander Field Command, DNA ATTN: FCPR FCTMOF Kirtland AFB, NM 87117
1	Commander Field Command, DNA Livermore Branch ATTN: FCPRL P.O. Box 808 Livermore, CA 94550
1	HQDA DAMA-ART-M Washington, DC 20310
10	Central Intelligence Agency Office of Central Reference Dissemination Branch ATTN: Room GE-47 HQS Washington, DC 20502
1	Program Manager US Army BMD Program Office ATTN: John Shea 5001 Eisenhower Avenue Alexandria, VA 22333
2	Director US Army BMD Advanced Technology Center ATTN: CRDABH-X CRDABH-S Huntsville, AL 35807

DISTRIBUTION LIST

No. of Copies — Organization

1 Commander
US Army BMD Command
ATTN: BDMSC-TFN/N.J. Hurst
P.O. Box 1500
Huntsville, AL 35807

1 Commander
US Army Engineer Division
ATTN: HNDED-FD
P.O. Box 1500
Huntsville, AL 35807

2 Deputy Chief of Staff for Operations and Plans
ATTN: Technical Library
Director of Chemical & Nuc Operations
Department of the Army
Washington, DC 20310

3 Commander
US Army Engineers
Waterways Experiment Station
ATTN: Technical Library
Jim Watt
Jim Ingram
P.O. Box 631
Vicksburg, MS 39180

1 Commander
US Army Materiel Command
ATTN: AMCDRA-ST
5001 Eisenhower Avenue
Alexandria, VA 22333-0001

3 Commander
Armament R&D Center
US Army AMCCOM
ATTN: SMCAR-TDC
SMCAR-TSS
W. Reiner
Dover, NJ 07801

1 Commander
US Army Armament, Munitions and Chemical Command
ATTN: SMCAR-ESP-L
Rock Island, IL 61299-7300

No. of Copies — Organization

1 Director
Benet Weapons Laboratory
Armament R&D Center
US Army AMCCOM
ATTN: SMCAR-LCB-TL
Watervliet, NY 12189

1 Commander
US Army Aviation Research and Development Command
ATTN: AMSAV-E
4300 Goodfellow Boulevard
St. Louis, MO 63120

1 Director
US Army Air Mobility Research and Development Laboratory
Ames Research Center
Moffett Field, CA 94035

1 Commander
US Army Communications - Electronics Command
ATTN: AMSEL-ED
Fort Monmouth, NJ 07703

1 Commander
US Army Communications - Research and Development Command
ATTN: DRSEL-ATDD
Fort Monmouth, NJ 07703

1 Commander
U.S. Army Communications - Electronics Command (CECOM)
CECOM R&D Technical Library
ATTN: AMSEL-IM-L, B 2700
Fort Monmouth, NJ 07703-5000

2 Commander
US Army Electronics Research and Development Command
ATTN: DELEW-E, W. S. McAfee
DELSD-EI, J. Roma
Fort Monmouth, NJ 07703-5301

DISTRIBUTION LIST

No. of Copies	Organization
7	Director US Army Harry Diamond Labs ATTN: Mr. James Gaul Mr. L. Belliveau Mr. J. Meszaros Mr. J. Gwaltney Mr. Bill Vault Mr. R. J. Bostak Dr. W. J. Schuman, Jr. 2800 Powder Mill Road Adelphi, MD 20783
4	Director US Army Harry Diamond Labs ATTN: DELHD-TA-L DRXDO-TI/002 DRXDO-NP DELHD-RBA/J. Rosado 2800 Powder Mill Road Adelphi, MD 20783
1	Commander US Army Missile Command Research, Development and Engineering Center ATTN: AMSMI-RD Redstone Arsenal, AL 35898
1	Director US Army Missile and Space Intelligence Center ATTN: AIAMS-YDL Redstone Arsenal, AL 35898-5500
2	Commander US Army Natick Research and Development Center ATTN: DRXRE/Dr. D. Sieling STRNC-UE/J. Calligeros Natick, MA 01762
1	Commander US Army Tank Automotive Research and Development Command ATTN: AMSTA-TSL Warren, MI 48397-5000

No. of Copies	Organization
1	Commander US Army Foreign Science and Technology Center ATTN: Rsch & Cncepts Br 220 7th Street, NE Charlottesville, VA 22901
1	Commander US Army Logistics Management Center ATTN: ATCL-O, Mr. Robert Cameron Fort Lee, VA 23801
3	Commander US Army Materials Technology Laboratory ATTN: Technical Library DRXMR-ER, Joe Prifti Eugene de Luca Watertown, MA 02172
1	Commander US Army Research Office P.O. Box 12211 Research Triangle Park NC 27709
4	Commander US Army Nuclear & Chemical Agency ATTN: ACTA-NAW MONA-WE Technical Library LTC Finno 7500 Backlick Rd, Bldg. 2073 Springfield, VA 22150
1	Commander US Army TRADOC ATTN: DCST&E Fort Monroe, VA 23651
2	Director US Army TRADOC Systems Analysis Activity ATTN: LTC John Hesse ATAA-SL White Sands Missile Range NM 88002

DISTRIBUTION LIST

No. of Copies	Organization
2	Commandant US Army Infantry School ATTN: ATSH-CD-CSO-OR Fort Benning, GA 31905
1	Commander US Army Development & Employment Agency ATTN: MODE-TED-SAB Fort Lewis, WA 98433
1	Commandant Interservice Nuclear Weapons School ATTN: Technical Library Kirtland AFB, NM 87115
1	Chief of Naval Material ATTN: MAT 3323 Department of the Navy Arlington, VA 22217
2	Chief of Naval Operations ATTN: OP-03EG OP-985F Department of the Navy Washington, DC 20350
1	Chief of Naval Research ATTN: N. Perrone Department of the Navy Arlington, VA 22217
1	Director Strategic Systems Projects Ofc ATTN: NSP-43, Tech Library Department of the Navy Washington, DC 20360
1	Commander Naval Electronic Systems Com ATTN: PME 117-21A Washington, DC 20360
1	Commander Naval Facilities Engineering Command Washington, DC 20360
1	Commander Naval Sea Systems Command ATTN: SEA-62R Department of the Navy Washington, DC 20362
3	Officer-in-Charge(Code L31) Naval Constr Btn Center Civil Engineering Laboratory ATTN: Stan Takahashi R. J. Odello Technical Library Port Hueneme, CA 93041
1	Commander David W. Taylor Naval Ship Research & Development Ctr ATTN: Lib Div, Code 522 Bethesda, MD 20084
1	Commander Naval Surface Weapons Center ATTN: DX-21, Library Br. Dahlgren, VA 22448-5000
2	Commander Naval Surface Weapons Center ATTN: Code WA501/ Navy Nuclear Programs Office Code WX21/Tech Library Silver Spring, MD 20902-5000
1	Commander Naval Weapons Center ATTN: Code 533, Tech Lib China Lake, CA 93555-6001
1	Commander Naval Weapons Evaluation Fac ATTN: Document Control Kirtland AFB, NM 87117
1	Commander Naval Research Laboratory ATTN: Code 2027, Tech Lib Washington, DC 20375

DISTRIBUTION LIST

No. of Copies	Organization
1	Superintendent Naval Postgraduate School ATTN: Code 2124, Technical Reports Library Monterey, CA 93940
1	AFSC/SDOA Andrews Air Force Base MD 20334
1	ADTC/DLODL, Tech Lib Eglin AFB, FL 32542
1	AFWL/SUL Kirtland AFB, NM 87117
1	Air Force Armament Laboratory ATTN: AFATL/DLODL Eglin AFB, FL 32542-5000
1	AFESC/RDCS ATTN: Paul Rosengren Tyndall AFB, FL 32403
1	AFATL (DLYV) Eglin AFB, FL 32542
1	RADC (EMTLD/Docu Libray) Griffiss AFB, NY 13441
1	AFWL/NTES, R. Henny Kirtland AFB, NM 87117-6008
1	AFWL/NTED, J. W. Aubrey Kirtland AFB, NM 87117-6008
2	Commander-in-Chief Strategic Air Command ATTN: NRI-STINFO Lib Offutt AFB, NB 68113
1	AFIT (Lib Bldg. 640, Area B) Wright-Patterson AFB Ohio 45433
1	FTD/NIIS Wright-Patterson AFB Ohio 45433

No. of Copies	Organization
1	Director Lawrence Livermore Lab. ATTN: Tech Info Dept L-3 P.O. Box 808 Livermore, CA 94550
2	Director Los Alamos Scientific Lab. ATTN: Doc Control for Rpts Lib P.O. Box 1663 Los Alamos, NM 87544
2	Director Sandia Laboratories ATTN: Doc Control for 3141 Sandia Rpt Collection L. J. Vortman P.O. Box 5800 Albuquerque, NM 87185
1	Director Sandia Laboratories Livermore Laboratory ATTN: Doc Control for Technical Library P.O. Box 969 Livermore, CA 94550
1	Director National Aeronautics and Space Administration Scientific & Tech Info Fac P.O. Box 8757 Baltimore/Washington International Airport MD 21240
1	Director NASA-Ames Research Center Applied Computational Aerodynamics Branch ATTN: MS 202-14, Dr. T. Holtz Moffett Field, CA 94035

DISTRIBUTION LIST

No. of Copies	Organization
3	Aberdeen Research Center ATTN: N.H. Ethridge J. Keefer Library P.O. Box 548 30 Diamond Street Aberdeen, MD 21001
1	Aerospace Corporation ATTN: Tech Info Services P.O. Box 92957 Los Angeles, CA 90009
1	Agbabian Associates ATTN: M. Agbabian 250 North Nash Street El Segundo, CA 90245
1	The BDM Corporation ATTN: Richard Hensley P.O. Box 9274 Albuquerque International Albuquerque, NM 87119
1	Black & Veach Consulting Engineers ATTN: H. D. Laverentz 1500 Meadow Lake Parkway Kansas City, MO 64114
1	The Boeing Company ATTN: Aerospace Library P.O. Box 3707 Seattle, WA 98124
1	California Research & Technology, Inc. ATTN: F. Sauer Suite B 130 11875 Dublin Blvd Dublin, CA 94568
1	California Research & Technology, Inc. ATTN: M. Rosenblatt 20943 Devonshire Street Chatsworth, CA 91311
1	Carpenter Research Corporation ATTN: H. Jerry Carpenter Suite 424 904 Silver Spur Road Rolling Hills Estates, CA 90274
1	Dynamics Technology, Inc. ATTN: D. T. Hove Suite 300 21311 Hawthorne Blvd. Torrance, CA 90503
1	Goodyear Aerospace Corporation ATTN: R. M. Brown, Bldg 1 Shelter Engineering Litchfield Park, AZ 85340
6	Kaman AviDyne ATTN: Dr. R. Reutenick (4 cys) Mr. S. Criscione Mr. R. Milligan 83 Second Avenue Northwest Industrial Park Burlington, MA 01830
3	Kaman Sciences Corporation ATTN: Library P. A. Ellis F. H. Shelton 1500 Garden of the Gods Road Colorado Springs, CO 80907
2	Kaman-TEMPO ATTN: DASIAC Don Sachs P.O. Drawer QQ 816 State Street Santa Barbara, CA 93102
1	Kaman-TEMPO ATTN: E. Bryant, Suite UL-1 715 Shamrock Road Bel Air, MD 21014
1	Lockheed Missiles & Space Co. ATTN: J. J. Murphy, Dept. 81-11, Bldg. 154 P.O. Box 504 Sunnyvale, CA 94086

DISTRIBUTION LIST

No. of Copies	Organization
1	Martin Marietta Aerospace Orlando Division ATTN: G. Fotiko P.O. Box 5837 Orlando, FL 32805
2	McDonnell Douglas Astronautics Corporation ATTN: Robert W. Halprin K.A. Heinly 5301 Bolsa Avenue Huntington Beach, CA 92647
1	New Mexico Engineering Research Institute (CERF) ATTN: J. Leigh P.O. Box 25 UNM Albuquerque, NM 87131
2	Physics International Corporation 2700 Merced Street San Leandro, CA 94577
2	R&D Associates ATTN: Technical Library Allan Kuhl P.O. Box 9695 Marina del Rey, CA 90291
1	R&D Associates ATTN: G.P. Ganong P.O. Box 9330 Albuquerque, NM 87119
2	Science Applications, Inc. ATTN: W. Layson John Cockayne PO BOX 1303 1710 Goodridge Drive McLean, VA 22102
1	Science Applications, Inc. ATTN: Technical Library 1250 Prospect Plaza La Jolla, CA 92037
1	Sparta, Inc. ATTN: I. B. Osofsky Suite 250, 23293 So. Pointe Dr. Laguna Hills, CA 92653
1	Sverdrup Technology, Inc. ATTN: R. F. Starr P. O. Box 884 Tullahoma, TN 37388
1	SRI International ATTN: Dr. G. R. Abrahamson 333 Ravenswood Avenue Menlo Park, CA 94025
2	Systems, Science and Software ATTN: C. E. Needham Lynn Kennedy PO Box 8243 Albuquerque, NM 87198
3	Systems, Science and Software ATTN: Technical Library R. Duff K. Pyatt PO Box 1620 La Jolla, CA 92037
1	Texas Engineering Experiment Station ATTN: Dr. D. Anderson 301 Engineering Research Center College Station, TX 77843
1	Thermal Science, Inc. ATTN: R. Feldman 2200 Cassens Dr. St. Louis, MO 63026
1	TRW - Ballistic Missile Division ATTN: H. Korman, Mail Station 526/614 P.O. Box 1310 San Bernadino, CA 92402

DISTRIBUTION LIST

No. of Copies — Organization

2 TRW Systems Group
ATTN: Benjamin Sussholtz
Stanton Fink
One Space Park
Redondo Beach, CA 90278

1 Battelle Memorial Institute
ATTN: Technical Library
505 King Avenue
Columbus, OH 43201

1 California Institute of Technology
ATTN: T. J. Ahrens
1201 E. California Blvd.
Pasadena, CA 91109

2 Denver Research Institute
University of Denver
ATTN: Mr. J. Wisotski
Technical Library
PO Box 10127
Denver, CO 80210

1 Massachusetts Institute of Technology
Aeroelastic and Structures Research Laboratory
ATTN: Dr. E. A. Witmer
Cambridge, MA 02139

1 Massachusetts Institute of Technology
ATTN: Technical Library
Cambridge, MA 02139

1 Northrop University
ATTN: Dr. F. B. Safford
5800 W. Arbor Vitae St.
Los Angeles, CA 90045

2 Southwest Research Institute
ATTN: Dr. W. E. Baker
A. B. Wenzel
8500 Culebra Road
San Antonio, TX 78228

1 Stanford University
ATTN: Dr. D. Bershader
Durand Laboratory
Stanford, CA 94305

Aberdeen Proving Ground

Dir, USAMSAA
ATTN: AMXSY-D
AMXSY-MP, H. Cohen

Cdr, USATECOM
ATTN: AMSTE-TO-F

Cdr, CRDC, AMCCOM
ATTN: SMCCR-RSP-A
SMCCR-MU
SMCCR-SPS-IL

USER EVALUATION SHEET/CHANGE OF ADDRESS

This Laboratory undertakes a continuing effort to improve the quality of the reports it publishes. Your comments/answers to the items/questions below will aid us in our efforts.

1. BRL Report Number _____ Date of Report _____

2. Date Report Received _____

3. Does this report satisfy a need? (Comment on purpose, related project, or other area of interest for which the report will be used.) _____

_____

_____

4. How specifically, is the report being used? (Information source, design data, procedure, source of ideas, etc.) _____

_____

_____

5. Has the information in this report led to any quantitative savings as far as man-hours or dollars saved, operating costs avoided or efficiencies achieved, etc? If so, please elaborate. _____

_____

_____

6. General Comments. What do you think should be changed to improve future reports? (Indicate changes to organization, technical content, format, etc.)

_____

_____

_____

CURRENT ADDRESS

_____
Name

_____
Organization

_____
Address

_____
City, State, Zip

7. If indicating a Change of Address or Address Correction, please provide the New or Correct Address in Block 6 above and the Old or Incorrect address below.

OLD ADDRESS

_____
Name

_____
Organization

_____
Address

_____
City, State, Zip

(Remove this sheet along the perforation, fold as indicated, staple or tape closed, and mail.)